



Review

Polymer crystallization of ultrathin films on solid substrates

Yi-Xin Liu, Er-Qiang Chen^{*,1}

Beijing National Laboratory for Molecular Sciences, Department of Polymer Science and Engineering and Key Laboratory of Polymer Chemistry and Physics of Ministry of Education, College of Chemistry, Peking University, Beijing 100871, China

Contents

1. Introduction	1011
2. Structure and morphology	1013
2.1. Edge-on and flat-on lamellae	1013
2.2. Morphology diagram	1021
3. Crystallization kinetics	1025
3.1. Primary nucleation	1025
3.2. Crystal growth	1026
4. Metastability of monolayer lamellae	1030
4.1. Thickening behavior	1030
4.2. Kinetics of monolayer lamellar thickening	1033
5. Summary	1036
Acknowledgements	1036
References	1036

ARTICLE INFO

Article history:

Received 30 December 2009

Accepted 13 February 2010

Available online 20 February 2010

Keywords:

Ultrathin film

Polymer crystallization

Morphology

Crystal growth

Thickening

ABSTRACT

Recently, polymer crystallization in ultrathin films (thickness less than 100 nm) on solid substrates has attracted increased attention. As it can be considered to be a quasi-two-dimensional (2D) system with one-dimensional (1D) confinement along the substrate normal, ultrathin polymer film offers unique possibilities for testing the theories of crystallization and for studying the effects of confinement and interface which may invoke new mechanisms other than those applied in bulk crystallization of polymers. In this article, we will summarize the important results of ultrathin film crystallization of polymers obtained in the past decades. The morphologies, the crystallization kinetics, and the transformation between monolayer crystals with various metastabilities are reviewed in depth, with an attempt at discussing the ultrathin polymer film crystallization in the general framework of thermodynamics and kinetics of crystallization.

© 2010 Elsevier B.V. All rights reserved.

1. Introduction

Ordering and crystallization of polymeric chains with regular chemistry structure is one of the most striking phenomena in condensed matter physics [1,2]. The process of polymer crystallization is a transition from a randomly coiled state to a perfectly ordered state. During this process a hierarchy of ordered structure develops, which in turn controls the physical properties of the polymer materials. In bulk, spherulites are the most common superstructures observed when crystallizing from melt, while single crystals

and dendrites can be grown from dilute solutions. Since the discovery of platelet single crystals by Keller [3], Till [4], Fischer [5], and the others [6] at the later 1950s, the concept of folded-chain crystal has been widely accepted. Actually, these lamellar crystalline structures with its one dimension only several or tens of nanometers, referred to as lamellae, are the basic unit of crystalline polymer substances, of which spherulites and other polycrystalline aggregate are composed.

As one of the most important forms of polymer matter, folded-chain crystals are non-equilibrium structures that trapped in metastable states with a significant degree of disorder, mainly characterized by the degree of chain folding [7]. Much effort has been devoted to understanding the molecular mechanism of forming this basic form of polymer crystals. Despite many thermodynamic considerations in the early years and a few recent discussions on

* Corresponding author. Tel.: +86 10 62753370; fax: +86 10 62753370.

E-mail address: eqchen@pku.edu.cn (E.-Q. Chen).

¹ For the PKU special issue.

nucleation, there is now a wide agreement that the structure of the polymer crystals is governed by kinetic rather than equilibrium factors [8]. Kinetically, the crystal growth rate results from the competition between the thermodynamic driving force which is related to the supercooling and a free energy barrier for crystallization. Moreover, the resulting growth rate is a function of lamellar thickness. Kinetic theories further assume that the thickness corresponding to the maximum growth rate on the lateral growth surfaces is chosen to grow macroscopic lamellae. The two most successful kinetic theories on polymer crystallization are the surface nucleation model formulated by Lauritzen and Hoffman (LH) [9–11], and the more recent entropic barrier model proposed by Gilmer and Sadler (GS) [12,13]. Both are based on the consideration of kinetic processes on the lateral growth faces thus belong to secondary nucleation theories (growth theories). It is the explanation of the origin of the barrier that differentiates these two models. In the LH model, an energy barrier is considered and it must be overcome via a random fluctuation as a molecule or a segment of a long chain attaches itself to the crystal growth front. However, the GS model argues that in addition to any free energy terms, the slowing down of attachment of a long segment onto a growth front is caused by exploring many possible configurations, only a few of which are favorable to grow further. Therefore, the barrier of GS model is largely entropic in nature. The LH model has been the most popular theory since its birth and it has been widely utilized to quantitatively fit experimental results because it is analytical and easy to apply, though more and more observations that cannot be explained by the LH model have been reported. The most recent progress in polymer crystallization comes from the study of the early stages of polymer crystallization [14]. It has been proposed that crystallization is preceded by an ordered precursor, which is either induced by a spinodal-assisted mechanism [15,16] or assumed to be a mesomorphic phase on the crystal growth front [17–19]. Since a detailed discussion of polymer crystallization in bulk is beyond the scope of this review, interested readers can refer to literature for further information, and in particular, a very recent book by Cheng [7] treating polymer crystallization as a phase transition involving metastable states is highly recommended.

Recently, polymer crystallization under spatial confinement, especially in thin (thickness less than 1000 nm) and ultrathin (thickness less than 100 nm) films on solid substrates, has attracted increasing attention [20]. The objective to study polymer crystallization confined in ultrathin films is twofold: (i) to develop new technologies and to enhance device performance, (ii) to provide new evidence to better understand the nature of polymer crystallization. On the one hand, polymer thin films have many potential applications in the field of molecular electronics, optics, sensors, and solar cells. It is possible to alter the properties of these devices via changing the degree of confinement and different interfaces. On the other hand, the morphology, crystallization kinetics, melting temperature, and other physical properties of individual lamellar crystals can be probed both in situ and real time in thin films in contrast to the averaged information obtained in bulk. It offers unique possibilities for testing theory. The molecular pathway during crystallization is expected to be directly monitored and there is indeed some progress in this area [21]. Moreover, as thin polymer films can be considered as a one-dimensional (1D) confinement system, it is of great interest to study the effects of confinement and interface. The chain orientation, segmental mobility, transporting process, and surface free energy at the interface which are usually neglected in bulk may become dominant factors in thin films. Therefore, new mechanisms other than those applied in bulk crystallization of polymers may be invoked.

A thin film on a substrate is subject to 1D confinement along the normal of substrate. Other examples of the 1D confinement are free standing films, lamellar phases of block copolymers,

and nanolayer assemblies created by a layer-multiplying coextrusion method. On the substrates, polymer crystallization in almost all types of polymer systems, from most conventional semicrystalline homopolymers such as polyethylene (PE) or *n*-alkane [22–26], poly(ethylene oxide) (PEO) [27–33], poly(*di*-*n*-hexane) (PDHS) [20,34], polypropylene (PP) [35–38], isotropic polystyrene (*i*-PS) [39–41], poly(3-hydroxybutyrate) (PHB) [42–45], poly(butylene adipate) (PBA) [46], poly(ethylene succinate) (PES) [47], poly(butylene succinate) (PBS) [48], poly(*L*-lactide) (PLLA) and poly(*D*-lactide) (PDLA) [49–54], poly(ϵ -caprolactone) (PCL) [53,55–58], poly(vinylidene fluoride) (PVDF) [59], poly(3,4-ethylenedioxythiophene) (PEDOT) [60], poly(ethylene 2,6-naphthalate) (PEN) [61,62], poly(trimethylene 2,6-naphthalate) (PTN) [63], poly(ethylene terephthalate) (PET) [64–66], and poly(trimethylene terephthalate) (PTT) [67], semicrystalline copolymers such as poly(bisphenol A alkyl ether) (BA-*Cn*) [68–71], poly(vinylidene fluoride-*co*-trifluoroethylene) (P(VDF-TrFE)) [72], poly(ethylene-vinyl acetate) (EVA) [73], and poly(*L/D*-lactide) [52], and polymer blends with more than one crystallizable component such as PCL/poly(vinyl chloride) (PVC) [74], PLLA/PDLA [52], PLLA/poly(ethylene glycol) (PEG) [50], PEO/PMMA [75–80], PEO/poly(arylene sulfone oxide) (PASO) [81], and PEO/polybutadiene (PB) [81], to block copolymers with one or more crystallizable blocks such as PS-*b*-PEO [82,83], PLLA-*b*-PS [84,85], PLLA-*b*-PEG [86], PEO-*b*-PB [87–89], poly(2-vinylpyridine) (P2VP)-*b*-PEO [90], poly(high-1,4-butadiene)-*b*-poly(styrene-*r*-butadiene) [91], and poly(high-1,4-butadiene)-*b*-poly(high-3,4-isoprene) [91], and semicrystalline polymer brushes grown from the substrates [92], have been studied extensively. Almost every aspect of polymer crystallization usually discussed for bulk systems, including morphology, kinetics, and metastability, have been addressed and some new crystallization habits have been discovered.

The film thickness that characterizes the degree of confinement and the substrate that controls the strength of substrate/polymer interface interaction are two most important parameters in thin film systems. The aforementioned categorization of thin and ultrathin films in terms of thickness is somewhat arbitrary. The change of some physical properties, such as molecular orientation and morphology, behaves discontinuously with decrease of film thickness. According to Ma et al., film thickness can roughly be classified into three categories [93]. The first category includes those films thicker than several hundred nanometers (usually termed as thin film). There, spherulites or lamellar bundles are usually observed and predominantly edge-on lamellae (with chain axis parallel to the substrate) are found. In the second category, the film thickness is less than 100 nm but larger than the coil size of polymers (usually termed as ultrathin film), wherein both edge-on and flat-on lamellae (with chain axis normal to the substrate) can form and typical morphologies are two-dimensional spherulites, seaweeds, dendrites, and multilayer lamellae with a spiral structure. The third category includes film thickness down to the coil size (also termed as ultrathin film, but in this review the term of “monolayer” is used), approaching a quasi-two-dimensional (quasi-2D) state where diffusion may become the dominant parameter instead of surface nucleation during crystallization. Thus, in monolayers the crystals usually grow with typical diffusion-limited morphologies, such as seaweeds and dendrites. In the literature, the term “thin film” sometimes refers to all films with thickness below 1000 nm. To avoid ambiguity, hereafter, thin film, ultrathin film, and monolayer, are used to exactly correspond to the three categories, respectively. It is worth mentioning here that some other physical properties are also significantly affected when reducing film thickness, but they change without discontinuities. Examples are crystallinity, crystallization kinetics, and optical and electronic properties such as conductivity.

While the size effect related to film thickness has been widely investigated in the literature, fewer experiments concerning the substrate effect have been carried out, mainly due to the lack of various kinds of atomic flat substrates with different surface properties and the difficulty to tune surface properties of the substrate continuously and freely. A further difficulty arises from the fact that it is really hard to split the substrate effect from size effect because they often couple together. Therefore, understanding of the substrate effect on the structure and molecular dynamics at the interface is still rudimentary. However, it is believed that interactions between substrate and polymers should play an important role on crystallization behavior. Several authors have reported a great depression of melting temperature when single crystals on substrate were heated, of which the degree of depression depends on the surface free energy of the substrate [25,94]. It is suggested that two classes of substrates can be identified, namely sticky wall and slippery wall, which correspond to strong attractive and repulsive force at the substrate/polymer interface, respectively [93]. Surely, whether the substrate is sticky or slippery will also depend on the polymer thereon.

Various techniques, including transmission electron microscopy (TEM) and electron diffraction (ED), scanning electron microscopy (SEM), atomic force microscopy (AFM), optical and polarized optical microscopy (OM and POM), grazing incidence wide angle X-ray diffraction (GIWAXD) and grazing incidence small-angle X-ray scattering (GISAXS), reflection high energy electron diffraction (RHEED), grazing incidence reflection absorption Fourier transform infrared spectroscopy (RA-FTIR), and dielectric spectroscopy (DS), have been employed to study the crystallization of polymer ultrathin films on solid substrates for last two decades. The real space imaging methods (TEM, SEM, AFM, and POM) are usually used to probe morphology, surface properties, crystallization kinetics, and melting behavior, while the others can detect the crystalline lattice, lamellar orientation, segmental and chain mobility, crystallinity and crystallization kinetics, and melting temperature. Among all above mentioned techniques, AFM as a non-destructive technique with its ability to obtain nanoscale structural information of soft materials both in situ and at real time in different environments is perhaps the most important and powerful one. The application of AFM since the early 1990s has led to a real change in our understanding of many fundamental processes. In particular, tapping-mode AFM (TM-AFM) coupled with a hot stage is quite suitable for monitoring crystallization processes of a wide variety of polymers in a wide temperature range. It has been extensively applied to investigate the crystalline morphology and the morphology evolution when subject to isothermal crystallization, melting, or annealing. Some quantitative data such as lamellar thickness and lamellar growth rate of various semicrystalline polymers can be obtained. Much detailed information concerning individual crystal lamella in ultrathin film which is hard to be detected by other techniques becomes accessible with the aid of TM-AFM. As the main focus of this review is the morphology and crystallization kinetics of monolayer lamellae on substrate, we will largely discuss the experimental results collected by TM-AFM.

In this review, we mainly focus on the topics of lamellar orientation transition, morphology diagram, crystallization kinetics in thin films, and the transformation between crystals (particularly monolayers) with various metastabilities. Although these aspects will be reviewed separately, we intend to put the different experimental and simulation observations and explanations suggested in literature in the framework of general crystallization theory. As we will emphasize below, the morphology of lamellar crystals grown in thin polymer films is still determined by both nucleation step and crystal growth step in non-equilibrium condition. The growth kinetics can be either nucleation- or diffusion-limited; and for the thin film case, particular attention should be paid to the diffu-

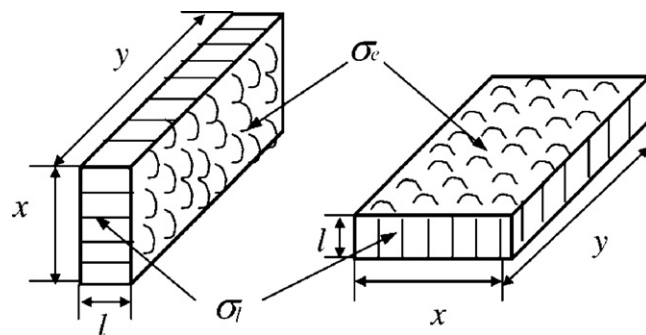


Fig. 1. Illustration of edge-on (left) and flat-on (right) lamellae. Note that the normal of the basal planes is either parallel to (edge-on) or normal to (flat-on) the substrate surface. The lamellar thickness is denoted as l and the other two dimensions are denoted as x and y , respectively. For edge-on lamellae, the dimension x is further constrained by the film thickness. The free surface energy of fold surface σ_e is usually much larger than that of lateral surface σ_l . Figure is reproduced from ref. [25] with modified expressions for surface energies.

sion of chains. The transformation between lamellae with different metastability is also expected to accommodate with classical nucleation theory, of which the late stage may be described by Ostwald ripening mechanism in general. On the other hand, we also intend to clearly demonstrate that the film systems provide unique opportunities to deepen our understanding of complex crystallization behaviors of polymer.

2. Structure and morphology

2.1. Edge-on and flat-on lamellae

Despite the presence of confinement and the substrate, semicrystalline polymers can crystallize in a conventional manner whereby polymer chains fold back and forth into stems to form lamellae. One of the greatest differences between polymer lamellae and small molecule single crystals is the anisotropy of their surface structures. As shown in Fig. 1, polymer lamellae are bounded by two basal surfaces covered by chain folds and several lateral surfaces. Although the exact structure of the fold surface, which may differ according to how the lamellae are formed, is not clear at present [95], it is believed that chain folds are mainly in amorphous or quasi-amorphous state in contrast to the lateral surface of polymer lamellae and the fully crystallized faces of small molecule single crystals. Therefore, the surface energy of the fold surface is quite different from that of the lateral surface: the former is generally ten times larger than the latter, which is much stronger than the differences among different crystalline faces of small molecule single crystals. In bulk, the anisotropic lamellae can isotropically distribute. However, for the thin films with thickness reduced to the lamellar thickness or to a small multiple of it, the anisotropic surface properties will eventually take effect because lamellae cannot rotate freely in 1D confinement space. As a result, preferential lamellar orientations should be produced in ultrathin films. Indeed, the preference of lamellar orientations is widely confirmed by experiments and has emerged as one of the hot spots in polymer crystallization of ultrathin films. Generally, two preferred orientations are encountered mostly in experiments: perpendicular (edge-on lamellae) and at the other extreme parallel (flat-on lamellae) to the substrate surface. Fig. 1 schematically shows these two orientations. Lamellar orientations are different from chain orientations. The lamellar orientation is the orientation of the normal of the basal planes, while chain orientation is not always parallel to the normal of the basal planes [96]. When the chain axis is parallel to the normal of the basal planes, chain orientation and lamellar orientation are the same. Questions in the literature concern

what controls the lamellar orientation and how. In this section we first give a summary of experimental observations and then review some theoretical models.

Before that, it is helpful to give a brief introduction on how to identify edge-on and flat-on lamellae in experiments. In most cases, by using imaging methods such as AFM, TEM, and OM, lamellar orientation can be easily recognized through morphology. Edge-on lamellae are usually in fibrous form with nearly uniform width, which aggregate further into axialites, hedrites, and spherulites, whereas flat-on lamellae may exhibit complicated patterns (dendrites, seaweeds) as well as regular forms (hexagons, squares, and lozenges) of faceted single crystals. Typical examples are given in Fig. 2 (more examples concerning different type of morphology can be found in Fig. 11). Sometimes it is very difficult to tell whether the lamellae are edge-on or flat-on only from the morphology. For instance, the lamella in Fig. 2c is actually a single crystal with flat-on orientation, indicated by the sharp diffraction spots in ED pattern, although its morphology is very similar to the spherulite shown in Fig. 2a where edge-on lamellae are packed together forming a polycrystalline structure. Therefore, ED is a powerful technique to confirm the lamellar orientation. Besides, GIWAXD and RA-FTIR are also adopted to evaluate lamellar orientation in thin and ultrathin films [27]. In GIWAXD, the lamellar orientation is determined by a crystal orientation function f_c which is derived from the angle between polymer main chain direction and the normal of the sample film. The lamellar orientation gradually changes from edge-on to flat-on when the value of orientation order parameter f_c ranges from -0.5 to 1.0 , and $f_c = 0$ indicates a random orientation. RA-FTIR is used as a complementary technique that can reveal the local-

ized chain structure near the substrate. The electric field of the infrared radiation reflected by the substrate is perpendicular to the film surface provided that the film thickness is sufficiently thinner compared to the wavelength of the incident infrared radiation. Thus, vibration modes having transition moments perpendicular to the film surface will appear with greater intensity than modes with parallel orientation. Edge-on lamellae can be distinguished from flat-on lamellae from the decrease of RA-FTIR intensity of modes related to main chain vibrations. Other techniques like RHEED [97] and near edge X-ray absorption fine structure (NEXAFS) [25,73,98] are occasionally used by some researchers.

Film thickness and consequently the confinement effect is the most investigated factor that affects the preference of the lamellar orientation. On the one hand, edge-on lamellae are predominantly found in thin films. Typical examples are crystallizations of PCL in PCL/PVC blend films of ca. $10\ \mu\text{m}$ thickness [74], PET films with several hundred nanometers [100] and several micrometers [101], PP films about $1\ \mu\text{m}$ thickness [36], PEO films with thickness larger than $300\ \text{nm}$ [27], PTN films thicker than $200\ \text{nm}$ [63], PCL films of $120\ \text{nm}$ and $200\ \text{nm}$ thickness [57,102], BA-C n films with a thickness between 100 and $300\ \text{nm}$ [70,71,103,104], and isotactic PP films with a thickness of about $200\ \text{nm}$ [37,105,106]. It is also possible to preferentially grow edge-on lamellae even when the film thickness is much less than $100\ \text{nm}$ in some cases. Hu et al. observed that edge-on lamellae were grown on the sub-flat-on lamellae in a $45\ \text{nm}$ thick PDHS film [107]. Godovsky and Magonov reported that quasi-2D spherulites with sheaflike patterns were able to form from the dip-crystallized ultrathin films with a thickness of about $20\ \text{nm}$ [108]. Those spherulites are composed of aggregates of edge-on

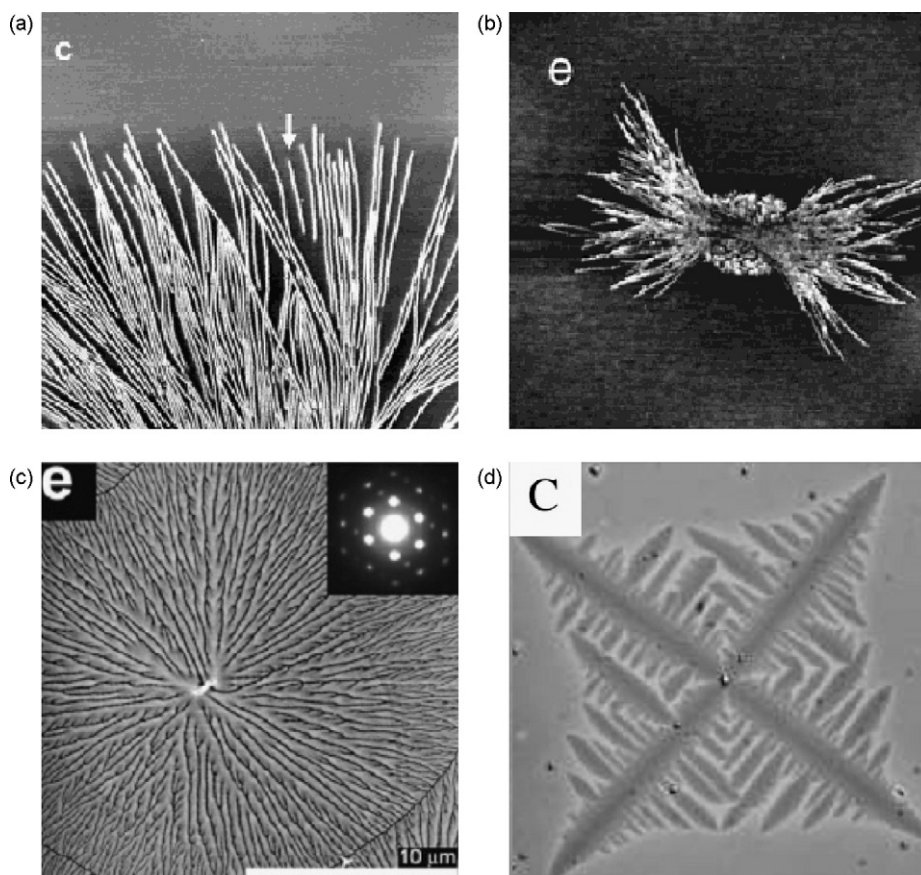


Fig. 2. The identification of lamellar orientation via morphology and ED pattern. Edge-on lamellae are usually observed in (a) spherulites with clear lamellar packing (only the border of the spherulite is shown), (b) axialites composed of single edge-on strands. Flat-on lamellae usually exist in (c) seaweeds, (d) dendrites. The inset of (c) shows the ED pattern which indicates flat-on orientation of the seaweed. Figures are reproduced from ref [99] for (a), ref. [70] for (b), ref. [57] for (c), and ref. [90] for (d), with permission of the copyright holders.

lamellae. The width of all above edge-on lamellae is of the order of 10 nm which is the typical thickness of polymer lamellae. However, as shown by Tracz et al. [109], much thicker edge-on lamellae can be produced via crystallization of PE at melt/HPOG interface, which is attributed to the mechanism of lamellar thickening growth.

On the other hand, flat-on lamellae are preferred in ultrathin films and monolayers. For crystallization of monolayers, the chance to find flat-on lamellae is exclusive. Reiter and Sommer [28] studied the crystallization of adsorbed PEO monolayers created via pseudodewetting and found that finger-like patterns with flat-on orientation were formed. The monolayer thickness after crystallization is between 5 and 10 nm as determined by AFM. The length of a fully extended chain (M_w of the PEO is 7600 g/mol) in crystalline state is 48 nm. Therefore, each molecule in monolayer lamellae folds more than five times. Later we [29] confirmed the pseudodewetting phenomenon with PEO ultrathin films on freshly cleaved mica substrates. Using X-ray reflectivity measurements, we determined the thickness of pseudodewetting layer of ~ 4.5 nm for the two PEO samples ($M_n = 4250$ g/mol and $M_n = 4700$ g/mol) with different chemistry of the chain ends. This liquid monolayer thickness is smaller than the coil size of PEO chains in melt (about 5 nm), implying that the chain conformation at least in the surface normal direction should be perturbed by the attraction force between PEO and the substrate. Similar results were obtained by other authors for PEO monolayers [30,31,110–112] as well as for PEO/PMMA blend monolayers [76–80]. In systematic studies on the crystallization of *i*-PS in ultrathin film with thickness less than 20 nm, Taguchi et al. [40,113] found that no matter what the morphologies were, the monolayer lamellae were always flat-on. Other similar results were reported in ultrathin films of PCL [57,102] and PDHS [107]. By

increasing film thickness to a small multiple of the coil size, without changing its orientation (flat-on), the morphology becomes more compacted, as observed in PEO ultrathin films with thicknesses between 17 and 120 nm [114] and up to 300 nm [27], in *i*-PS ultrathin films thicker than 30 nm [41,115], in PLLA ultrathin films with thickness of 20 and 50 nm [54] and of 500 nm [52], and in isotactic PP thin films with thicknesses of about 200 nm [37,105,106]. The flat-on crystals formed at large supercooling usually demonstrate much thinner fingers, leaving fewer and narrower gaps among fingers; at a very low supercooling, crystallization results in multilayer faceted single crystals.

According to all the above experimental information, a general trend is clearly revealed: decrease of film thickness gradually shifts the favor of edge-on orientation to flat-on orientation. The more the film thickness decreases, the more easily flat-on lamellae can be observed. However, an exact transition thickness was seldom reported. Keeping other conditions constant, Schönherr and Frank [27] reported that 300 nm was the transition thickness for PEO films on silicon wafers, whilst a transition thickness of 200 nm was determined for PTN films on silicon (1 0 0) and gold-coated silicon wafers [63]. The difference of transition thicknesses may be attributed to different polymer and substrate systems, different techniques applied to measure the thickness, or rather that a sharp transition point does not even exist. Indeed, by carefully examining experimental observations in literature, one may find that the transition from edge-on to flat-on orientation occurs in a broad range of thicknesses, and within the range there is a coexistence of edge-on and flat-on lamellae. Many authors have studied this transition process by varying film thickness [25,57,63,73,92,102,107,116,117], but few of them focused on the transition region of the film thickness.

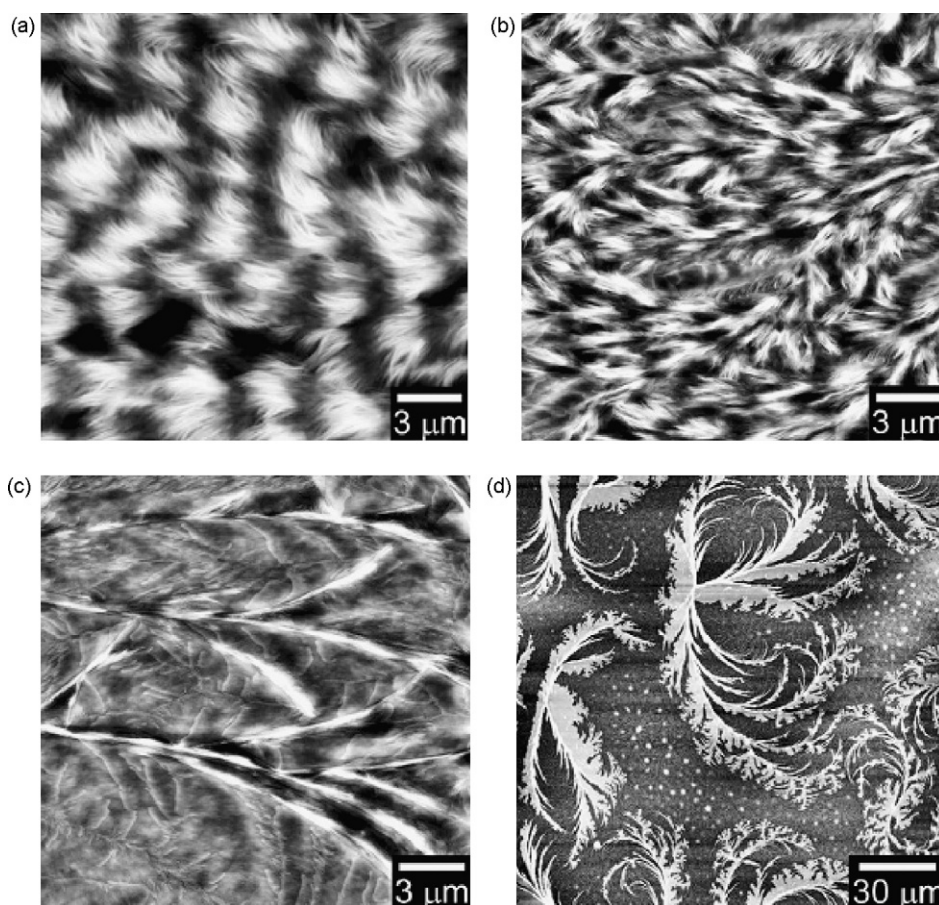


Fig. 3. Film thickness dependence of lamellar orientation by contact mode images of the LLDPE films with thicknesses of (a) 370, (b) 194, (c) 126, (d) 21 nm fully crystallized at 115 °C. The concentration of edge-on lamellae decreases gradually from (a) to (d). Figures are reproduced from ref. [116], with permission of the copyright holders.

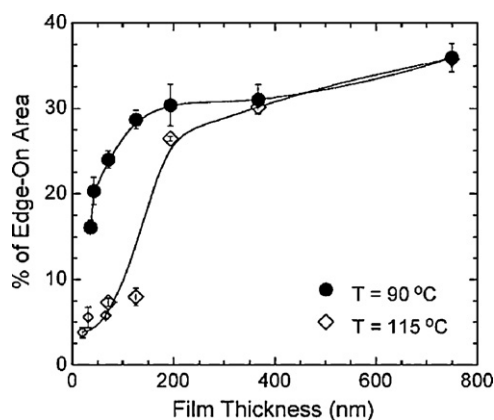


Fig. 4. Ratio of area of edge-on lamellae to total area for films isothermally crystallized typically for 2 h. The ratio is obtained from threshold and histogram of AFM images. The ratio decreases with film thickness and the ratio of films crystallized at a high temperature is much bigger than films crystallized at a low temperature for same thicknesses in the smaller region of thicknesses. Figure is reproduced from ref. [116], with permission of the copyright holders.

Most recently, Jeon and Krishnamoorti [116] carried out a systematic study on the film thickness dependence of lamellar orientation. To study the effect of film thickness only, they purposely fabricated a series of thin and ultrathin linear low-density PE (LLDPE) films with thickness ranging from 20 to 800 nm on etched silicon wafers by spin-coating method. The isothermal crystallization was conducted after all prior thermal history was erased by a pre-melting procedure. The morphologies of these crystallized films were observed by contact mode AFM. A typical sequence of images is shown in Fig. 3. As the film thickness decreases, the morphology varies from banded spherulite with regular undulations (Fig. 3a) to sheaflike morphologies (Fig. 3d) with two intermediate structures (Fig. 3b and c). Accompanying with the variation of morphologies, the fraction of edge-on lamellae is reduced accordingly, as shown in Fig. 4. A similar trend of this transition is also identified by Liang et al. using GIWAXD and RA-FTIR techniques [63], which is demonstrated either by the turnover of the signs of crystal orientation function (Fig. 5a) or by the decrease of absorbance ratio (Fig. 5b). Interestingly, the transition thickness for LLDPE films crystallized at 115 °C and that for PTN films crystallized at 160 °C are both around 200 nm. However, it should be taken as a coincidence, because the transition thickness seems to depend on crystallization temperature. As can be seen from Fig. 4, the transition thickness for LLDPE

films crystallized at 90 °C is smaller than the thickness for films crystallized at 115 °C.

A simple thermodynamic model was proposed by Wang et al. [73] to explain the preference of lamellar orientation in crystallization of polymer films. The free energies of formation were first calculated for edge-on and flat-on nucleus by assuming a specific shape and both contacting with substrate. Then the critical dimensions for edge-on and flat-on nucleus were obtained through minimizing the two free energies, respectively. Finally, the critical energy of nucleation for forming both types of nucleus were readily calculated using critical dimensions. The result shows that as long as the surface free energy of crystal/substrate interface is smaller than that of melt/substrate interface, the critical nucleation energy of edge-on nucleus is much lower than that of flat-on nucleus. Thus, the primary nuclei favor edge-on orientation. When the film is thick enough, it is assumed that the growth of lamellae is more likely to take the same orientation of the primary nuclei which is edge-on so as to avoid creating new interfaces. Therefore, the model explains why edge-on orientation is preferred in thick films. The situation becomes different in ultrathin films and monolayers, as edge-on lamellae would create much more interface areas than the continuous flat-on lamellae for they must be packed together in a geometrically confined space. Thus, edge-on orientation is no longer thermodynamically favorable and flat-on lamellae are predominantly observed. However, this simple model cannot explain some critical experimental observations. For example, it is impossible to explain the appearance and disappearance of embryos observed by Lei et al. [68] and Schönherr et al. [38]. The surviving embryos are indeed primary nuclei and must be formed at or near the film surface, because if they were grown from the edge-on nuclei formed at the polymer/substrate interface, they would become stable after they touched the film surface so they would not disappear. More importantly, this thermodynamic model is insufficient to describe the decrease of the fraction of edge-on lamellae with decrease of film thickness and the coexistence of two types of lamellae with different orientations. In fact, the coexistence of edge-on and flat-on orientation forces one to conclude that the reorientation is a kinetic process rather than an equilibrium case. In addition, this model assumes that there is no difference of surface free energy between fold surface and lateral surface of lamellae, meaning that the anisotropic feature of polymer lamellae is neglected. The validity of this model is not fully examined yet.

To improve the understanding of the effect of film thickness on lamellar orientation, Chan and co-workers recently proposed a

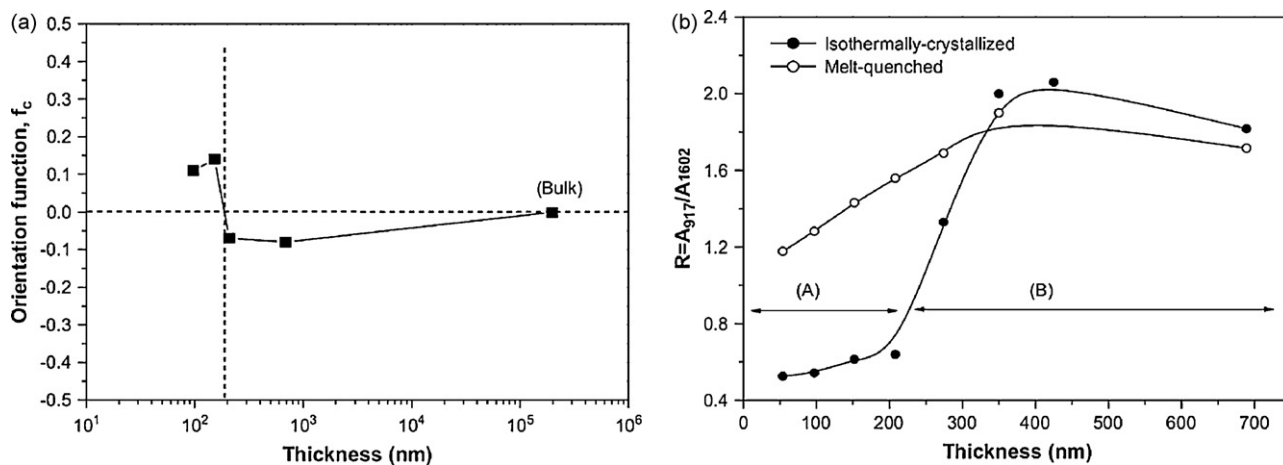


Fig. 5. (a) The crystal orientation function calculated from GIWAXD results of isothermally crystallized PTN films as a function of film thickness. (b) Absorbance ratios of the 917 cm^{-1} and 1602 cm^{-1} band as functions of film thickness using RA-FTIR. Both figures show that the lamellar orientation shift from edge-on to flat-on with decrease of film thickness. Figures are reproduced from ref. [63], with permission of the copyright holders.

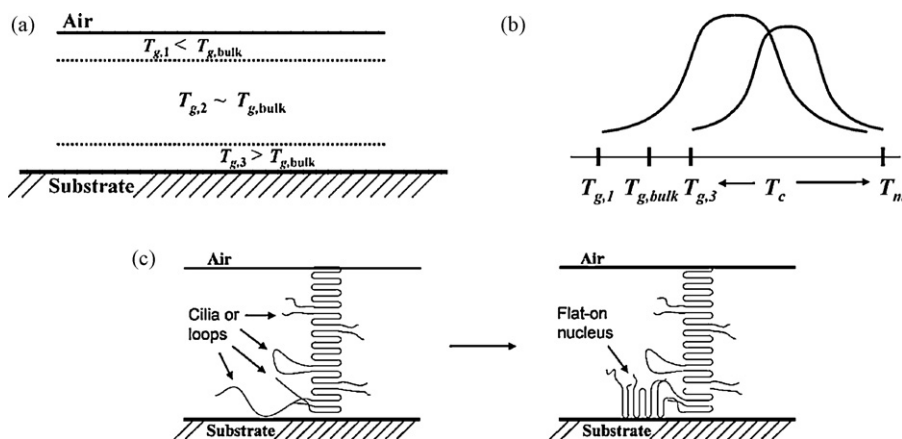


Fig. 6. (a) Schematic showing of the three-layer model for a polymer/substrate system. (b) Bell shaped curves for the nucleation rates of the polymer in the layer with $T_g = T_{g,1}$ near the film surface (left) and $T_g = T_{g,3}$ near the substrate surface (right). (c) Illustration of the formation of an induced flat-on nucleus at the polymer/substrate interface linked to an edge-on lamella. Figures are reproduced from ref. [117], with permission of the copyright holders.

three-layer model [117]. There, in addition to nucleation effects, kinetic effects are also incorporated. Firstly, the nucleation effects are considered. It is well-known that the local chain (segmental) mobility or glass transition temperature (T_g) of a thin film varies as a function of depth into the sample. In particular, they consider that the free surface region causes a local enhancement of dynamics that leads to reduction of the T_g value, and the substrate retards the segmental mobility resulting in an increase of the T_g value. These two effects produce three layers of polymers with different T_g s in thin films. Fig. 6a gives a schematic showing of the three-layer model for a polymer thin film. The relation of T_g s of three layers is $T_{g,1} < T_{g,2} < T_{g,3}$, where $T_{g,1}$, $T_{g,2}$, and $T_{g,3}$ is the T_g of the layer of free surface, the middle layer or bulk, and the layer of polymer/substrate interface, respectively. In polymer crystallization, it is well established that the plot of the primary nucleation rate as a function of temperature bears a peak almost centered in the temperature range of T_g and T_m , and exhibits a overall bell shape. Since the T_g s of the free surface layer and the polymer/substrate interface layer are different, a significant shift of the peak value of the primary nucleation rate for these two layers is expected, as shown in Fig. 6b. This difference suggests that the nucleation at the free surface is favored under low temperatures, while the nucleation near the polymer/substrate interface is faster under high temperatures. Illuminated by the simple thermodynamic model, Chan and co-workers assume that nucleation of flat-on lamellae are preferred at the polymer/substrate interface. (Note that the constraint of this assumption is much weaker than that of the thermodynamic model where the film thickness needs to be sufficiently thin to make flat-on orientation favorable.) But, unlike the simple thermodynamic model, they argue that the nucleation of edge-on lamellae occurs only at the free surface. It is believed that the much smaller surface energy of lateral surface (Fig. 1) than that of the fold surface is the main reason why edge-on orientation is preferred at the free surface. Combining all above nucleation mechanisms together, the three-layer model predicts that edge-on lamellae will predominant at low temperatures close to T_g while flat-on lamellae will be preferred at high temperatures approaching to T_m . This crystallization temperature dependence of lamellar orientation is noticed by some authors and will also be discussed later on.

After the consideration mentioned above, Chan and co-workers introduced kinetic effects. When crystallized at intermediate temperatures, nucleation of edge-on and flat-on lamellae both can occur in appreciable rates so that they will compete with each other. If the film is not too thick, edge-on lamellae nucleated at the free surface can propagate to the substrate in a short time and meanwhile flat-on lamellae nucleated at the polymer/substrate

interface can grow to the free surface. Therefore, there should be a coexistence of edge-on and flat-on lamellae when observed by surface imaging techniques. Furthermore, when the edge-on lamellae touch the substrate, loose loops and protruding cilia attaching to the substrate may induce additional formation of flat-on nuclei, as shown schematically in Fig. 6c. The fast growth of these nuclei and other flat-on lamellae will eventually lead to the enclosure of edge-on lamellae if a much faster growth rate of flat-on lamellae than that of edge-on lamellae is assumed. As the film thickness increases, it will need much longer time for flat-on lamellae initially on the substrate to grow upwardly to the free surface. The melt near the free surface region will be exhausted by the growth of edge-on lamellae, which have originated at the free surface, before flat-on lamellae propagate to this region. Thus, an increase of the concentration of edge-on lamellae with increase of film thickness can be predicted by the three-layer model. Even at high temperatures, where the nucleation rate of edge-on lamellae is much slower than the nucleation rate of flat-on lamellae, edge-on lamellae will be predominantly observed at least near the film surface. Most of above predictions agree well with experimental observations.

Although the three-layer model improves our understanding of the effects of film thickness as well as crystallization temperature on the preferential lamellar orientation phenomenon, it is only qualitative, and says nothing of how many the value of T_g will vary from the film top surface to the substrate surface. It is unable to obtain the exact transition thickness using this model in the present version. Much work has to be done before it can predict the experimental results quantitatively. To achieve a quantitative description of this model, the effects of film thickness and crystallization temperature must first be delineated. In the case of lack of quantitative description, the results containing information not only at the film surface but also in whole film using GIWAXD and RA-FTIR measurements cannot be explained directly in the context of three-layer model. According to three-layer model, when the film is thick enough and the temperature is high, flat-on lamellae have no chance to appear at the free surface due to kinetic limitations. However, the fraction of flat-on lamellae can overwhelm the fraction of edge-on lamellae since the nucleation rate of flat-on lamellae is much higher than that of edge-on lamellae. Consequently, despite the abundance of edge-on lamellae at the free surface, flat-on lamellae should still be predominant in the whole film. Then, the transition thickness obtained via techniques probing whole film (GIWAXD, RA-FTIR) will be bigger than that obtained via surface imaging techniques (AFM) when crystallized at high temperatures. Or, no transition of lamellar orientation can be detected via GIWAXD or RA-FTIR. This phenomenon has not

been investigated yet. Another shortage of the three-layer model is that it cannot be readily extended to the case of none or repulsive interactions at polymer/substrate interface due to the fact that the strong attractive interaction is necessary for constructing the three layers with different T_g s.

As predicted by the three-layer model, crystallization temperature affects lamellar orientation in a similar way as film thickness does. With the increase of the temperature, a transition from edge-on lamellae to flat-on lamellae should occur. This prediction was confirmed by Chan and co-workers [117] and also by other authors [47,116] Fig. 7 shows a typical sequence of morphologies which change correspondingly with crystallization temperatures. The film thickness (33 nm) was purposely chosen by the authors to be close to the threshold thickness at which T_g began to dramatically increase by reducing film thickness. At very low temperature (45 °C), the image is filled with curved edge-on lamellae and no flat-on lamellae can be found. By raising the temperature to 60 °C, flat-on lamellae appear in the matrix of edge-on lamellae, although they are both small and scarce. At higher temperatures, more and more flat-on lamellae develop until they totally cover the whole image area at 90 °C. These results clearly demonstrate that low temperature favors edge-on lamellae, while high temperature prefers flat-on lamellae. Jeon and Krishnamoorti [116] reported a similar result, although only two temperatures, one close to the melting temperature and the other much lower, were investigated. Fig. 4 shows the ratio of area of edge-on lamellae to the total area they measured from recorded images. As expected, the ratio at 90 °C is higher than that obtained at 115 °C when film thickness is less than 200 nm. However, when the film thickness exceeds 200 nm where banded spherulites were formed, the fraction of edge-on lamellae was comparable at both crystallization temperatures. Another demonstration of the effect of temperature on lamellar orientation was given by Yuryev et al. [52]. In crystallization of PLLA thin films (about 500 nm thick), they observed that the transition from edge-on lamellae to flat-on lamellae was coupled with an interesting transformation of morphology, from non-oriented stacks, perfect 2D spherulites, axialites, to truncated lozenge morphology.

It is well known that molecular weight (or chain length) is a very important parameter in polymer crystallization, especially for low molecular weight polymers [8]. It is possible that when crystallized at a certain temperature, only higher molecular weight polymers can crystallize while lower molecular weight polymers is still in liquid state. In other words, the supercooling (also the driving force for crystallization) of higher molecular weight polymers is larger than that of lower molecular weight polymers, although they are under the same crystallization temperature. Thus, it can be expected that molecular weight will also significantly affect lamellar orientation just like crystallization temperature does. Unfortunately, none of investigations concerning this effect for polymers has been reported. The study of molecular orientation of crystalline ultrathin films of linear alkanes with different chain length may give some hints [98]. Fu and Urquhart studied the molecular orientation of thin films of two *n*-alkanes, *n*-C₆₀H₁₂₂ (HC) and *n*-C₃₆H₇₄ (HTC) by NEXAFS spectroscopy. The results show that the longer chain molecules prefer to lie down on the substrate (analogue to edge-on orientation), while the shorter chain molecules tend to stand on the substrate with methyl group at the substrate surface and chain backbone normal to the substrate (analogue to flat-on orientation). The authors explained this phenomenon by considering the free energy associated with different molecular orientations. The methyl group favors locating at the substrate surface due to the lower surface free energy of the methyl group compared to the methylene group. Therefore, the “flat-on” orientation of *n*-alkanes on substrate should be the equilibrium configuration. However, as the alkane molecules were deposited to the substrate in a non-equilibrium condition where alkanes were supercooled, the stronger enthalpic interaction of HC with NaCl surface relative to HTC should hold HC molecules laterally oriented on the substrate. With reducing the chain length or with increasing temperature, “edge-on” molecules will gain enough energy to overcome the interaction with substrate and to orient “flat-on”. Thus, “edge-on” orientation is kinetically preferred. Although the case of polymers should be more complicated due to the folding of long chain molecules, both the stronger enthalpic interaction and dilution of

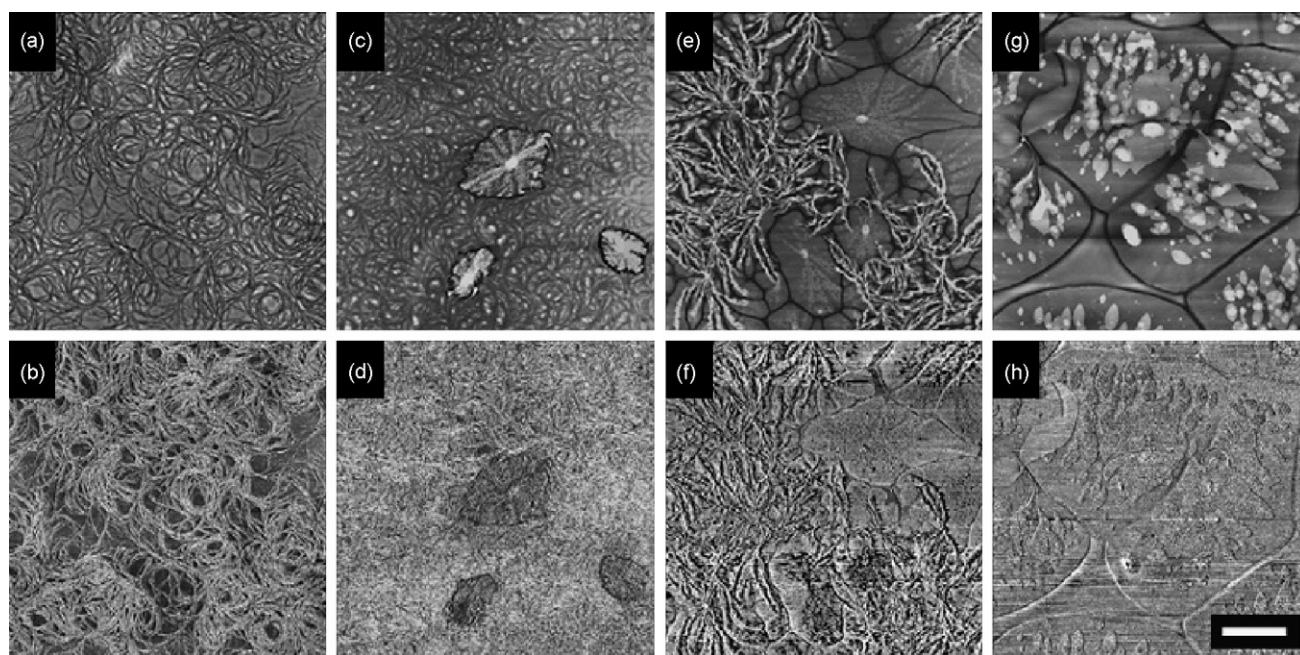


Fig. 7. A set of height (upper row) and the corresponding phase (bottom row) AFM images shows the crystalline morphologies of poly(bisphenol A hexane ether) (BA-C6) films with thicknesses of about 33 nm crystallized at 45 (a and b), 60 (c and d), 75 (e and f), and 90 °C (g and h) for 84 h. As the crystallization temperature increases, flat-on lamellae (large smooth regions) become more and more prominent. The scale bar in (h) indicating a length of 10 μm is applicable to all presented images. Figures are reproduced from ref. [117], with permission of the copyright holders.

chain ends will cause the favor of edge-on orientation for higher molecular weight polymers. From this point of view, the effect of crystallization temperature can also be explained in this way. Another implication is that end group effect cannot be ignored for low molecular weight polymers. If there is much stronger attractive interaction of end groups compared to backbone segments, flat-on orientation is the final equilibrium structure. Otherwise, if there is much stronger repulsive interaction of end groups than that of backbone segments, edge-on orientation is preferred. Note that final equilibrium orientation must not be the actual orientation because kinetic effects can play dominant role. All above speculations have not been intensively studied till now.

As can be seen from the above accounts, it is almost impossible to avoid considering the role of the interaction between polymers and substrate even when the studies intend to focus on other factors. Despite the importance of substrate effect, few results have been published. As an attempt to understand the microscopic origin of the dominance of flat-on lamellae in ultrathin films, Ma et al. [93] performed dynamic Monte Carlo (MC) simulations to study the crystallization kinetics as well as the molecular orientation for 128-mers. To elucidate the effect of the substrate, two kinds of substrate, namely sticky wall and slippery wall, linking to adhesive and repulsive interactions respectively, were investigated. They found that for slippery walls, edge-on lamellae were dominant at the whole range of crystallization temperature and film thickness they examined, while as to sticky walls, flat-on lamellae tended to dominate at high temperatures or at small film thickness. Surprisingly, these results are contrary to the case of crystallization of alkanes, wherein alkanes are often observed to prefer to lie down on the substrate due to the strong attraction between alkane backbone and the substrate [118]. In order to explore the origin of the preference of lamellar orientation in ultrathin films, the crystal growth of two orientations was studied via a so called self-seeding technique. The computer simulations show that the growth of edge-on lamellae is almost completely suppressed on sticky walls because the thickening of the lamellae at the lateral growth fronts is badly restricted by the frozen effect of sticky walls on the proximate segments, while growth of flat-on lamellae undergoes a limited retardation. Then, the authors claim that the dominance of flat-on lamellae can be related to the inhibited growth of edge-on lamellae due to the hindered thickening of lamellae at the lateral growth front. To this end, one may simply attribute the contradiction between polymer (128-mers) and alkane (15-mers to 50-mers) to much longer chain length of polymers compared to that of alkanes, because there is no need for short chain molecules to thicken to grow extended chain crystals. However, these results of MC simulations are also not supported by some experimental observations for polymers. Hu et al. [34] studied the morphology and structure of crystalline PDHS thin films and found that on the amorphous carbon coated mica (slippery wall), where there are weak van der Waals interactions between absorbed molecules and substrate, flat-on lamellae of PDHS were dominantly formed, while on HOPG (sticky wall), where there are strong van der Waals interactions at polymer/substrate interface, edge-on orientation for PDHS lamellae was preferred. They propose that the selection of orientation for lamellae as well as polymer chain is governed by the balance of absorbate-absorbate intermolecular interactions and molecules-substrate interactions. If intermolecular interactions exceed molecule-substrate interactions, as in the case of PDHS thin films on amorphous carbon coated mica surface, flat-on orientation is selected. By enhancing molecule-substrate interactions, polymer chains tend to lie down to gain more interaction energy. But, there are also some situations where experiments coincide with computer simulations. Wang et al. [25] observed a transition from edge-on to mainly flat-on lamellar orientation with decreasing film thickness when PE thin films were crystallized on silicon (1 1 1) wafers (Si), while for aluminum

coated silicon wafers (Al) and polyimide sheets (PI), only edge-on lamellae were observed in all film thicknesses. Since the surface free energy of PE/Si interface is smaller than that of PE/Al and PE/PI, Si substrate can be considered as a sticky wall and the other two are more close to slippery walls. These observations seem to agree quite well with the predictions of MC simulations. In addition, the fact that a transition of lamellar orientation occurs during varying film thickness for the same substrate also imply that one should not simply assign a lamellar orientation according to the properties of the substrate without considering other factors such as film thickness, temperatures, etc. The discrepancy between computer simulations and experiments indicates that the effect of substrate on the selection of lamellar orientation is still poorly understood.

Besides, other factors, such as sample preparation methods (spin-coating, drop-casting, dip-coating, melt-cast, vacuum deposition), solvent, non-crystalline block in block copolymers, and non-crystalline component in blends can also affect lamellar orientation. The way how thin films are prepared may not be critical, but attention should be paid to ensure that the experimental observations are reproducible. It is believed that non-crystalline blocks or components can alter the surface free energy at polymer/substrate interface. Through controlling the fraction of the non-crystalline block and the concentration of the non-crystalline component, one can adjust the surface free energy at polymer/substrate easily and continuously. Therefore, the effect of non-crystalline blocks or components may be mapped to the substrate effect. Moreover, the crystallization of crystalline block will additionally constrained by the microphase separation of block copolymers.

Remarkably, the transition of lamellar orientation not only occurs by varying above listed factors but also can take place when lamellae grow to some extent. The latter phenomenon was first clearly demonstrated by the work of Kikkawa et al. [53,54]. The PLLA thin film with 100 nm thickness premelted at 220 °C was isothermally crystallized at 160 °C and the whole crystallization process was in situ monitored by a temperature-controlled AFM. A typical set of time sequential images recorded by AFM is shown in Fig. 8. The first image is taken after crystallization for 10 min, in which only melt was observed. In Fig. 8b, an edge-on lamella has been nucleated. This lamella can propagate both parallel and perpendicular to film surface. Further growth of the lamella introduces some curvature (Fig. 8c). After crystallization for 21 min, edge-on lamella suddenly changes its orientation and a flat-on lamella is generated at the lower left growth tip of the lamella (Fig. 8d). Another flat-on lamella appears at the other growth tip as indicated by the white arrow in Fig. 8e. The two flat-on lamellae keep on growing to form approximately hexagonal crystals, while the growth of edge-on is totally impeded due to the enclosure of flat-on lamellae. The whole transition process happens under constant experimental conditions (film thickness, temperature, substrate and so on). In addition, the growth rates at the direction parallel to the film surface for edge-on and flat-on lamellae are almost the same. Based on these facts, one may conclude that the preference of lamellar orientation is mainly nucleation controlled. At the beginning of crystallization, the nucleation of edge-on lamellae is preferred. Consequently, edge-on lamellae are first observed. If flat-on nuclei are purposely added to the film as soon as the crystallization begins, they will definitely develop because they possess the same growth rate as edge-on lamellae do. Although it is much harder for flat-on lamellae to nucleate homogeneously at the film surface, they can nucleate easily at the growth tip of edge-on lamellae as revealed by experiments.

Kikkawa et al. have proposed a possible mechanism to explain the phenomenon mentioned above [53]. They assumed that several parts of molecular chains might not be incorporated and packed into the crystal lattice due to molecular inclination and chain shift in edge-on lamellae. As a result, loops and long cilia (amorphous chain

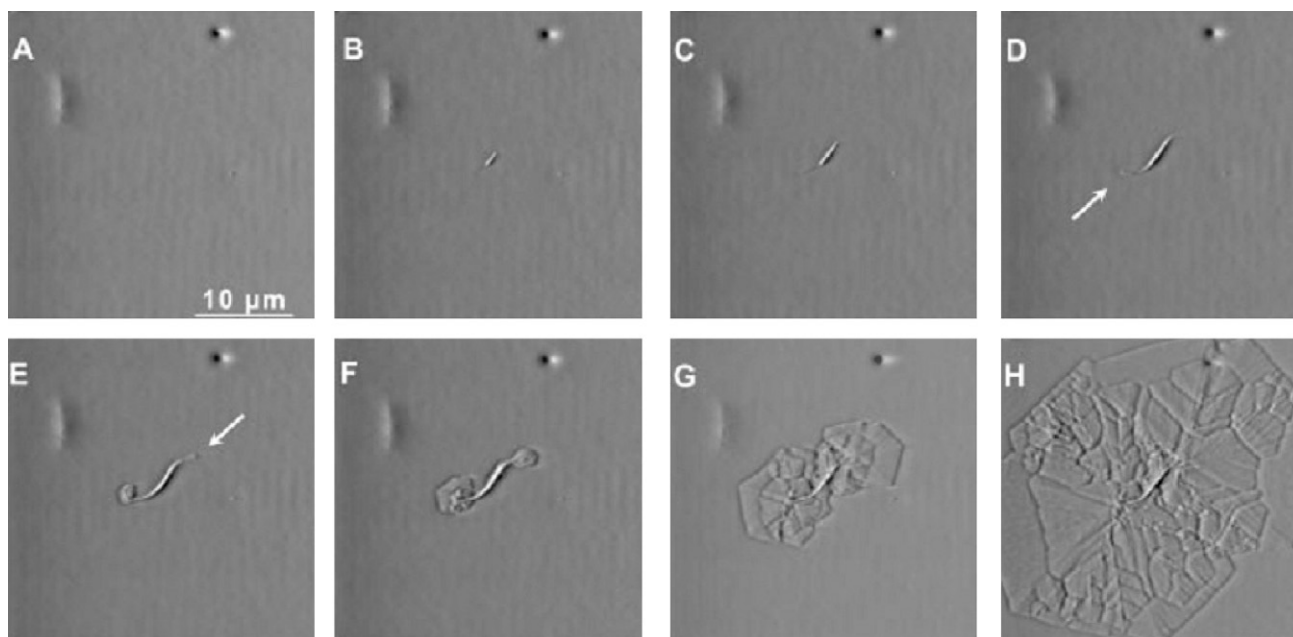


Fig. 8. A series of AFM deflection images of S-shaped edge-on crystal and hexagonal flat-on lamellar crystals in PLLA film during isothermal crystallization at 160 °C. The first frame (A) was taken at 10 min after the sample temperature was stable at 160 °C. The following images were recorded with an interval of about 3 min. Arrows in (D) and (E) indicate the flat-on lamellae developed from edge-on lamellae. Figures are reproduced from ref. [53], with permission of the copyright holders.

ends and repeating units close to them) should protrude on the crystal surface. These loops and cilia feel two constraints simultaneously. One is that they are covalently bonded to the crystal surface, resulting lower molecular mobility; and the other is that they are suppressed by the free surface/air interface to have chain direction perpendicular to the film surface. These constraints force the flat-on lamellae to nucleate on the parent edge-on lamellae. Thus, it is the constraints of crystal surface and air/polymer interface that make the nucleation of flat-on lamellae much easier compared to homogeneous nucleation at the surface. An alternative explanation was given by Jradi et al. [39]. They assumed that the nuclei formed at the growth tip of edge-on lamellae were randomly oriented, either flat-on or edge-on. On the basis of the fact revealed by their experiments that flat-on lamellae grow faster than edge-on lamellae, they expect that flat-on lamellae will eventually dominate and a transition from edge-on to flat-on orientation occurs. This mechanism is significantly different from the one proposed by Kikkawa et al. In this mechanism the crystal growth rather than nucleation is the controlling process. As a consequence of this mechanism, if edge-on lamellae grow faster than flat-on lamellae under certain circumstance and the orientation of nucleated lamellae is still randomly chosen, edge-on lamellae will branch out at the nucleation site to develop daughter edge-on lamellae instead of flat-on lamellae. This prediction was actually observed in the work of Li and co-workers [68,70]. There, an edge-on lamella was observed to breed more edge-on lamellae and to develop into a lamellar sheaf and finally into a spherulite. It is somewhat surprising that the branching phenomenon which is supposed to be one of the origins for forming spherulite can be fitted into current mechanism for understanding the transition of edge-on and flat-on orientation. To conclude, edge-on lamellae are preferentially nucleated at the film surface and nuclei with randomly chosen orientation are generated at the growth tip of the initial edge-on lamellae now and then. According to the relative growth rate of edge-on and flat-on lamellae, a transition of edge-on to flat-on or of edge-on to edge-on is expected.

Also, the transition from edge-on to flat-on can be found in the case of that edge-on lamellae are intentionally created by

rubbing or scratching amorphous polymer films using AFM tips [27,39,50,51,56]. In the study of Fujita et al. [56], PCL film with thickness of about 100 nm was first completely melted and then subjected to crystallize at various temperatures (46–54 °C). As shown in Fig. 9a, initially the film is featureless and no crystal is found. After the supercooled PCL film was scratched with AFM tip at the position indicated by the white dotted line, edge-on lamellae start to develop from the induction line, with its growth direction perpendicular to the line (Fig. 9b–d). The growth of edge-on lamellae is believed to be caused by the alignment of amorphous PCL chains in the scanning direction induced by the imposed shear stress. After a certain period of crystallization time, the lamellar orientation changes to flat-on manner at a distance from the induction line, as shown in Fig. 9e. Later on, flat-on lamellae keep on growing without further changing its orientation. It has been also found that the distance from induction line to the position where the change of lamellar orientation occurs depends little on crystallization temperature and molecular weight.

In contrast, Maillard and Prud'homme [50] reported that this distance was significantly affected by the crystallization temperature in PLLA films, as the density of edge-on lamellae decreased with temperature. They also claim that they have observed that flat-on lamellae could directly grow from induction line. Due to lack of high resolution images and information at initial time region, the assertion is not well supported because the length of initial edge-on lamellae may be too short to be recognized in low resolution images (one can compare Fig. 1 in ref. [51] to Fig. 2 in ref. [39]). A most recent study carried out by Jradi et al. has demonstrated that the transition from edge-on to flat-on lamellae could be highly reduced by changing hard scratching to soft rubbing, i.e. by reducing the load of AFM tip [39]. The authors raised a hypothesis that the conformation of polymer chains far from the scratched line (the order of hundreds of nanometers or even microns) was significantly perturbed due to the entanglement network originating from large chain length. If this hypothesis is true, there is higher possibility for hard scratching to induce the nucleation and growth of flat-on lamellae, and the effect of load of AFM tip is explained.

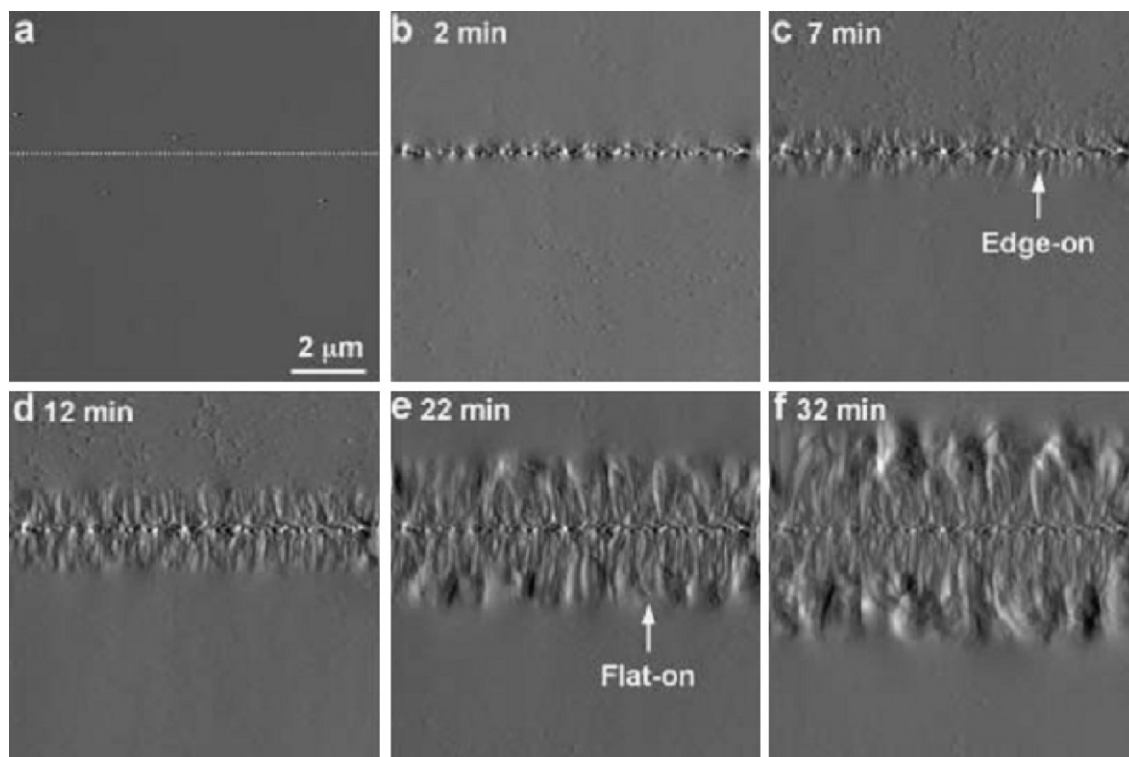


Fig. 9. AFM amplitude images of supercooled amorphous thin film and its AFM tip-induced crystallization of PCL ($M_n = 1.68 \times 10^5$ g/mol) at 50 °C. The dotted line in (a) indicates the scanning line with a strong, normal load ($A_s/A_f = 0.03$). The sequential images show that edge-on lamellae was induced by tip scratching and flat-on lamellae developed from them after edge-on lamellae grew to some extent. The image frame and the scanning rate were $10 \mu\text{m} \times 10 \mu\text{m}$ and 1.0 Hz ($20 \mu\text{m/s}$). Figures are reproduced from ref. [56], with permission of the copyright holders.

Intriguingly, while the transition from edge-on to flat-on lamellae was frequently observed, the transition of the opposite direction, i.e. from flat-on to edge-on lamellae, was rarely encountered. Yuryev et al. reported that flat-on lamellae could occasionally flip to edge-on lamellae when PLLA thin films were crystallized at a low supercooling [52]. Recently, Farrance et al. also observed a similar transition in crystallization of $1 \mu\text{m}$ thick PHB films and found that the growth of edge-on lamellae was much faster than flat-on lamellae [119]. The third example comes from the study of crystallization of a diblock copolymer PS-*b*-PEO in the presence of solvents [82]. It has been shown that solvent molecules at the polymer/substrate interface could sufficiently weaken the interaction between polymer and substrate, thus the original flat-on lamellae were no more favored and were changed to edge-on lamellae.

As a final remark in this section, in addition to the typical flat-on and edge-on orientations other orientations are also possible. For example, the twisting behavior may be invoked by the unbalanced surface free energy [7]. Due to the space limit of this review, the fascinating twisting lamellae grown from thin films, which deserve a careful analysis, will not be included here.

2.2. Morphology diagram

As mentioned in the previous section, the transition of lamellar orientation always accompanies changing morphologies in polymer thin films. Typical morphologies associated with edge-on orientation are spherulitic structures and those in flat-on manner are dendrites and seaweeds. With respect to the study of spherulitic structures in polymer thin films, recent interest has been focused on characterizing the fine structure of banded spherulite, a special class of spherulitic structure with lamellar twisting that shows a beautiful pattern of concentric rings seen under POM contrast to the

Maltess-cross pattern for normal spherulite, and on understanding the formation mechanism of both banded and non-banded spherulites, in particular, lamellar tip splitting and branching mechanisms [22,46,50,69,120,121]. For this progress we are largely in debt to the feasibility of AFM technique to monitor fine structures both in situ and in real space with nanoscale resolution. Although in these studies the thin film morphologies (film thickness is usually over 100 nm) are investigated, their structures are considered the same as in bulk so that the results obtained in thin films can be readily applicable to bulk case and confinement effect has been seldom concerned. Since the purpose of this review is to deal with the impact of introducing 1D confinement, we refer the interested readers to the original publications. Here we restrict ourselves to examining morphologies relating to flat-on orientations in ultra-thin films and in monolayers.

When polymeric materials form single crystals, they crystallize in a faceted manner. As discussed previously, the faceted crystals take the form of lamellae, which are single crystals with hexagonal, squared, and lozenged shapes, etc. The faceted manner that lamellae take corresponds to the equilibrium shape resulted from the anisotropy of either surface energy or kinetic coefficient inherited from the symmetry of crystalline lattice [122]. However, it has been shown that the presence of facets does not necessarily preclude pattern formation, a non-equilibrium growth process forming complex self-organized patterns. Pattern formation during crystallization, first intensively studied in metals and small molecules, has attracted increasing interest in polymer science. Recent studies of polymer crystallization in thin films have revealed a variety of non-faceted, non-equilibrium morphologies. The richness of non-equilibrium morphologies has brought about plenty confusions. For instance, the seaweed structure is sometimes called dense branching morphology (DBM), or referred to fractal structure, or termed as finger-like pattern. To clarify these confusions,

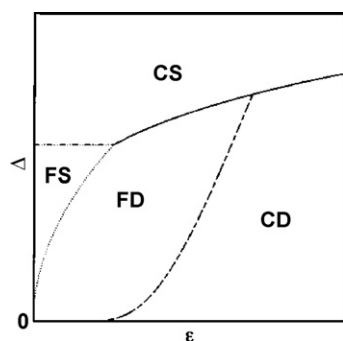


Fig. 10. BMT morphology diagram of possible structures for two-dimensional diffusion-limited growth. CS: compact seaweed; FS: fractal seaweed; CD: compact dendrite; FD: fractal dendrite. The figure is reproduced from ref. [125], with permission of the copyright holders.

a unified classification is highly required. Here, we adopt a classification scheme proposed by Brener et al. (BMT) [123]. The BMT classification uses two criteria that each reflect one of the most important features which are essential to describe the morphology. The first criterion is the pattern internal structure which is characterized by the fractal dimension (D_f). According to relative value of D_f , one may discriminate between the fractal (F) structures with $D_f < d$ with d being the space dimension, and compact (C) structures otherwise. A fractal pattern is one with a self-similar or self-affine internal structure. A true fractal can only be realized in a limit sense where the correlation length becomes infinite, which requires zero supercooling for crystallization, leading to zero growth rate of crystals. Under non-equilibrium conditions (with a degree of supercooling), fractal properties within a pattern may still exist over an intermediate range of length scales. Usually, a scaling range of at least one order of magnitude in length scales is required. Another classification criterion deals with the existence of geometrical order in the morphology. Morphology is called dendrite (D) if it has pronounced geometrical order; otherwise, the morphology is called seaweed (S). In this scheme, four distinct morphologies as being of type FD, FS, CD, and CS can be denoted accordingly.

Because similar patterns appear in crystal growth, viscous fingering, electrochemical deposition, and bacterial colony growth, the pattern formation seems to be independent of many of the details of specific experimental realizations, and people believe that common mechanisms underlying the pattern formation are existed. Remarkable progress of theoretical and numerical research has been made during the last thirty years, among which the theoretical framework devised by Brener et al. [123–126] seems to best agree with the results obtained in crystallization of polymer thin films. In the BMT theory, the supercooling Δ and the effective anisotropy ϵ of surface energy (crystalline anisotropy) are the two essential parameters. On the basis of a scaling argument with asymptotic matching requirements, solutions expected in some limits of the parameters could be recovered, and a morphology diagram, also called kinetic phase diagram in literature, was successfully constructed (see Fig. 10). The morphology diagram uses the supercooling and anisotropy as principle axes and discriminates between dendrites and seaweeds as the basic patterns. Dendrites can grow at arbitrary small Δ , but usually a finite amount of ϵ is required to produce highly oriented tips. Dendritic trunks (original branches) exhibit a smooth, approximately parabolic tip, which propagates without apparent change of shape. Sidebranches branch out oscillatory after the main trunk grows to some extent and grows in crystallographically favored directions away from the parent dendrite. By contrast, seaweeds do not require the anisotropy and is favorable for larger Δ and smaller ϵ .

The advancing growth front repeatedly bifurcates, generating a randomly branched pattern without apparent geometrical order. The transition between these two patterns occurs around the solid line ($\Delta \sim \epsilon^{1/4}$) in Fig. 10 which is continued by the dotted line. At small Δ and ϵ , the noise is expected to become important and induce tip splitting. Consequently, both seaweeds and dendrites may further change from compact to fractal, resulting in four morphology regions in morphology diagram. The noise induced length scale a_f is smaller than the tip radius ρ_t . In the range between a_f and ρ_t the structures are fractal with a nontrivial D_f ($D_f \approx 1.71$). This is one of the most important characteristics that differentiate fractal structures from compact ones. In the range between ρ_t and the diffusion length l_D , both fractal and compact structures are fractal but with a trivial fractal dimension $D_f = 3/2$. All morphologies become compact ($D_f = d$) as the length scales being larger than the diffusion length. In practical, one need to perform a series of measurements of fractal dimension on various length scales because a_f , ρ_t , and l_D are often unknown. Only if a fractal dimension being around 1.71 can be identified on a range of length scales, the fractal manner can be confirmed.

Within the framework of the BMT theory, most of morphologies and morphological transitions observed in crystallization of polymer thin films can be explained systematically. Fig. 11 shows a list of typical morphologies that are frequently encountered in experiments. Clearly, lamellar crystals in polymer thin films can exhibit whole spectrum of morphologies predicted by the BMT theory and an additional morphology with faceted habit. The envelope of dendritic structures usually displays a regular geometrical shape just like faceted crystals and sometimes the sides of the shape can be either concave or convex, indicating the underlying crystalline anisotropy. The seaweeds show an overall rounded shape without any favorable direction for tip growth. Although there are many irregular branches in compact seaweeds, the reported CS structures are almost exclusively single crystals in polymeric materials [78] (see Fig. 1c) in contrast to the cases of metals or small molecules [127]. The main element of the dendrite is a dendritic trunk with a parabolic tip, and the main element of the seaweed is a doublon which consists of two half tips and a groove between them (see Fig. 11a). For CS and CD structures, the tips of the dendritic trunk and doublon are stable against noise. Sidebranches which fill the space and make structures compact are triggered by the noise. For FS and FD structures, the noise is strong enough to destroy the dendritic trunk and doublon and fractal structures are resulted.

According to the morphology diagram, morphological transitions can take place by varying the supercooling, the anisotropy, or by varying supercooling and anisotropy together to generate a path in the diagram. Taguchi et al. have examined the supercooling dependence of morphology [40]. The *i*-PS single crystals were grown at several crystallization temperatures in ultrathin films (11 nm thick) and the corresponding surface topographies were recorded by AFM. Under a rather low supercooling (32 K or a crystallization temperature of 210 °C), a hexagonal single crystal bounded by six (110) crystallographic planes is observed. With increasing the supercooling, the 110 facets are no longer straight: they are first caved in at the middle point to form star-like structures (205 °C); then side branches appears at 200 °C forming snowflake-like dendrite; later the density of side branches increases but the whole shape remains hexagonal (195 °C and 190 °C); below 180 °C the six-fold symmetry is lost and the irregular tip splitting finally leads to the formation of a compact structure. In short, morphologies undergo changes from faceted single crystals, to CD structures, and then to CS structures with increasing supercooling, indicating that the growth of morphology is along the supercooling line at relatively high anisotropy in the right region of the BMT morphology diagram. Beers et al. also studied the

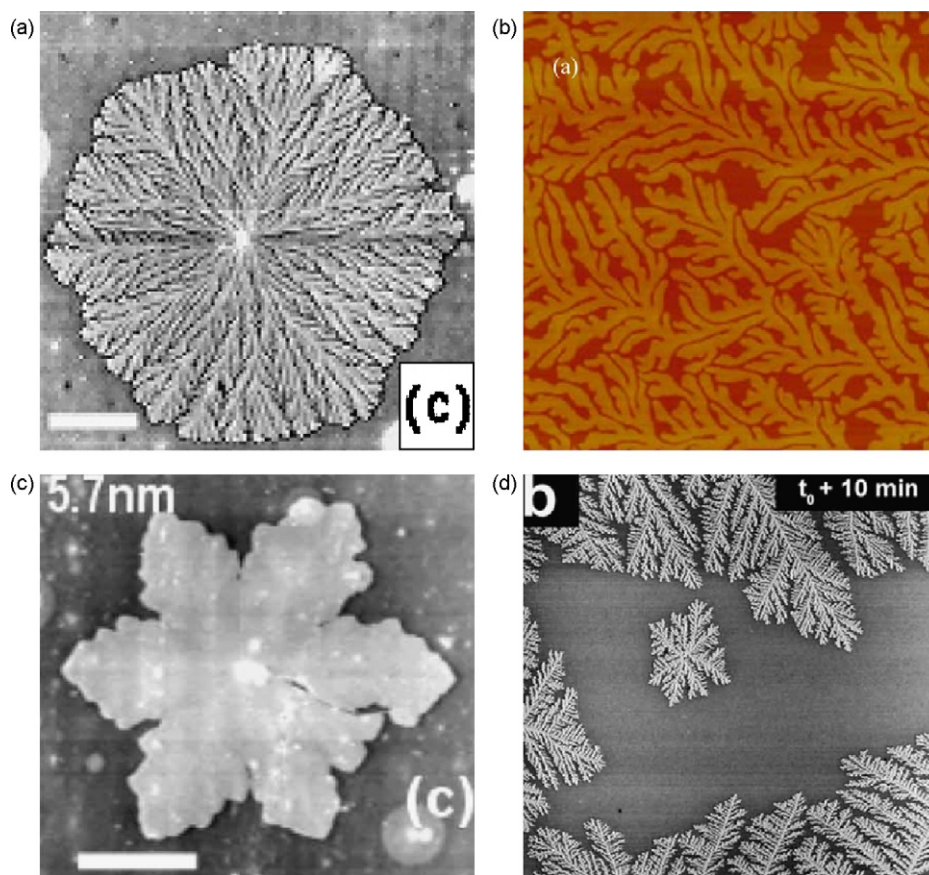


Fig. 11. Growth crystalline morphologies observed in polymer thin films. (a) Compact seaweed (CS) or DBM. (b) Fractal seaweed (FS) or finger-like structure. (c) Compact dendrite (CD) or symmetric dendrite. (d) Fractal dendrite (FD). Figures are reproduced from ref. [128] for (a), ref. [129] for (b), ref. [113] for (c), and ref. [58] for (d), with permission of the copyright holders.

crystallization in thin films of *i*-PS and observed a similar transition from CD to CS by varying temperatures [41]. Zhang et al. reported a similar transition from faceted single crystals to CD structures when an intermediate molecular weight PEO fraction was crystallized under various supercoolings on silicon wafers [112]. They also observed an additional CD to FD transition under higher supercoolings and lack of FD to CS transition. This observation suggests that the growth of morphology in this case occurs along the supercooling line at relatively low anisotropy in the middle part of the BMT morphology diagram where dendritic region is divided into FD and CD by the dashed line. The highest supercooling in their experiments probably does not reach the CS region. In all above observations and other unmentioned results [130,131], there is a common trend that the mean width or the mean separation size of branches decreases with increasing supercooling. Generally, diffusion-limited growth patterns are characterized by the diffusion length defined as $l_D \propto D/G$, where D is the diffusion coefficient and G is the tip growth rate. In crystallization of polymers, it is commonly accepted that D will decrease but G will increase with the supercooling. Consequently, l_D is reduced accordingly, resulting in smaller mean width of branches.

At a first look, one may simply conclude that this observation is fully consistent with the BMT morphology diagram except the faceted to dendritic transition which is not included in the diagram. However, the supercooling in melt crystallization of polymer thin films in fact does not directly relate to a diffusion field as the supercooling assumed in the BMT theory does. In the BMT theory, there is a gradient of concentration or a gradient of temperature at the growth front according to which kind of supercooling is considered. In crystallization of polymers, however, neither an

appreciable temperature gradient exists because the crystal growth is slow enough so that the heat can diffuse away from growth front quickly, nor need a concentration gradient be considered for the pure materials. By carefully inspecting their AFM images, Taguchi et al. have observed a gradient of film thickness of melt at the crystal growth front: the thickness of melt increases gradually with the distance away from the growth front and finally saturated to the uniform thickness of the liquid film. They conjecture that it is this gradient of film thickness that introduces the instabilities and an analogy between crystallization of polymer ultrathin films and that of solutions can be established. Here, the thickness of melt, which is proportional to the amount of polymer segment density (per unit area), is assumed to correspond to the concentration. It is imagined that the segment density decreases near the growth front as materials are consumed due to the fast surface kinetics and the slow mass transport process. Although the presence of impurity can also generate a concentration gradient, this idea seems more convincing and has been further confirmed by us [29] and Ma et al. [111]. Often, the term depletion zone is used to describe the thickness depression region and its width relate to the diffusion length. We reported that the presence of depletion zone was necessary to trigger diffusion-limited growth mechanism before the morphological instabilities set in on a micrometer length scale [29]. There, the concept of “2D solution”, which is quite similar to the diffusion-limited aggregation (DLA) model in which crystals grow from a gas with a finite density [122,132], was first demonstrated. Therefore, one may expect that the growth phenomenon in polymer thin films can be described by the DLA model with finite gas density. At present, it is still not clear how supercooling affects the diffusion field with a gradient of the segment density and thus leads to a

similar transition of morphology as described by the BMT morphology diagram. We hope the awareness of the connection between “2D solution” and DLA model with finite gas density may provide some new insights. In addition, Ma et al. has measured the width of depletion zone and found it was close to gyration radius of polymer chains on solid substrates in the particular case of crystallization of a high molecular weight PEO fraction in ultrathin films on silicon wafers [111]. This might provide a direct way to determine the diffusion length.

In addition to the morphology diagram, the 2D phase field simulation was also employed to study the supercooling dependence of selecting morphology. In the study of Xu et al. [133], similar to the BMT theory, the effect of supercooling and anisotropy on the formation and transition of morphology has been examined. By varying supercooling and anisotropy systematically in their phase field simulations, Xu et al. has established a morphological landscape similar to the BMT morphology diagram, wherein with increasing supercooling or decreasing anisotropy, the edges of faceted single crystal become unstable and the morphology undergoes changes from the highly ordered hexagonal shape to CD, and then to CS structure. Note that these phase field simulations were unable to produce fractal structures (FD and FS) mainly due to enormous separation of time scales associated with the surface kinetics and mass diffusion and due to the highly diffuse nature of the interfaces [76,127]. The theoretical and numerical studies of fractal structures are commonly based on the diffusion-limited aggregation (DLA) model [132,134–138]. Nonetheless, Taguchi et al.'s and other authors' observations were perfectly repeated by the simulation [40]. An interesting phenomenon discovered in simulations is that it is impossible to grow all kinds of morphologies by varying only supercooling as in experiments. The authors thus argue that the anisotropy must have some temperature dependence. If this hypothesis is valid, the anisotropy will vary with the supercooling and the morphology will pass the morphology landscape in a curved path. In a study of crystallization of a low molecular weight PEO fraction ($M_n = 5000$ g/mol) with ultra-narrow molecular weight distribution (PDI = 1.008), Zhai et al. observed a “reversed” transition that FS changes to FD with increasing supercooling [30]. This phenomenon is incompatible with BMT morphology diagram but can be readily understood by introducing the temperature dependence of anisotropy. Then the morphology can move along a curved path with the starting point at the low Δ and low ε of the FS region and end point at the high Δ and high ε of the FD region with increasing supercooling. In this context, however, a temperature gradient is considered to be responsible for producing instability other than the segment density gradient. If the segment density gradient is considered instead, a possible explanation is that a linear decrease of crystallization temperature may result a non-linear behavior of segment density gradient which can also draw a curved path on the BMT morphology diagram using segment density as Δ . If it is the case, the temperature dependence of anisotropy becomes unnecessary.

Contrast to supercooling, as ε has never been measured for high molecular weight polymers [75,76] experimentally, the effect of anisotropy is much harder to investigate compared to Δ and few results have been reported. In principle, ε can be determined from analysis of the mean tip radius of dendrites, the tip growth rate, the capillary length, and the diffusion coefficient, or from crystallization near equilibrium [75]. Despite the lack of the exact value of ε , Ferreira et al. reported a feasible method to tune the surface tension anisotropy by varying the composition of a polymeric blend, PEO/PMMA, which is composed of a crystallizable polymer (PEO) and a non-crystallizable polymer (PMMA) and these two components are completely miscible [75,76]. Upon crystallizing PEO component in thin films, they observed a transition of morphology from spherulite, to CS, then to CD, and finally to FD with

increasing PMMA concentration. Then a comparison between the observed crystal morphologies and those generated by a phase field model with the effective anisotropy varied by tuning the concentration of Cu component of Ni–Cu alloy has been made. A remarkable agreement for CS to CD transition is found, and the fact that the ε increases with PMMA concentration can be confirmed. Obviously, the transition from CS to CD can fit in the BMT morphology diagram quite well. While the CD to FD transition is not predicted by the phase field simulation, the authors suggest that the high viscosity of blend film with high PMMA concentration should have an impact on the stability of the growth tips, and moreover, the low concentration of PEO could also contribute to the noisy nature of the resulting FD patterns. In addition, the BMT morphology diagram is also incapable of explaining the CD to FD transition which occurs when ε is enhanced. Recently, Okerberg and Marand also explored the crystalline morphologies in crystallization of PEO chains mixed with PMMA in thin films [77,78]. Morphology maps, as functions of PMMA molar mass and crystallization temperature at different blend compositions, are constructed, to demonstrate the roles of the various controlling parameters. The general trend of CS to CD transition with increasing ε , i.e. PMMA concentration, can be extracted from the morphology maps ignoring two novel morphologies of needles and stacked needles. The comprehensive morphology maps may serve as a general guide for further studies of morphological transitions and growth kinetics as functions of supercooling, anisotropy and chain length of non-crystallizable component in certain morphology regime.

Besides Δ and ε , the effect of film thickness h on morphology selection has also been examined by several researchers [41,57,76,113,114,128]. Taguchi et al. reported the film thickness dependence of morphology of *i*-PS single crystals grown at 180 °C in ultrathin films with thicknesses between 4 and 20 nm [128]. The CS structures appear at large film thickness and change to the more open FD structures by reducing film thickness. At higher crystallization temperatures (190 °C and 195 °C), a transition from CD to FD occurs through decreasing film thickness [113]. Mareau and Prud'homme also observed that the CS structure of crystallization of 15 nm thick PCL films on silicon wafers could change to FD structure when the film thickness shrank to 6 nm [57]. Taguchi et al. suggest that the gradient of the film thickness should play an essential role in morphology instabilities and the selection of morphologies. But questions about how this gradient of the film thickness leads to morphological transition have not been addressed. Similar to the case of supercooling, the variation of the characteristic length of observed morphologies shows a common trend that the characteristic length increases and structures become more open as the film thickness decreases. This trend has been explained as that the characteristic length is of the order of diffusion length $l_D = D/G$. At a certain temperature, while the D keeps constant, the tip growth rate G is measured experimentally decrease with film thickness. However, the origin of film thickness dependence of G remains unclear.

To understand the h dependence of G , actually, one can get some hints from the idea of “2D solution” mentioned previously. In a numerical study of growing crystals from a gas with a finite density n_g , which is a sound analogy to “2D solution”, Uwaha and Saito [139] found that the aggregate growth rate and the gas density obey following relation for low n_g (<0.3),

$$G \propto n_g^{1/(d-D_f)}. \quad (1.1)$$

For high n_g , the speed of increase of G with n_g slows down; and a fractal to compact transition of morphology occurs when the increase of G deviates from Eq. (1.1). In “2D solution” of polymers on substrates, the analogue of gas density is the segment density which is the concentration of “2D solution”. Since h must be proportional

to the segment density, i.e. $h \propto n_g$, one can expect the following relation,

$$G \propto h^{1/(d-D_f)}, \quad (1.2)$$

where for the space dimension $d=2$, the typical value of D_f is 1.71 for fractal structures and is 1.5 for compact structures, respectively. Eq. (1.2) may give a general relation between G and h as $G \propto h^\nu$, where $\nu=1/(d-D_f)$ can vary from 2 (compact) to 3.45 (fractal). It predicts that the aggregate growth rate will increase as a power law with the film thickness, which qualitatively agrees with experimental results [90]. Moreover, the deviation of increase of G with h at high h region was also confirmed by Taguchi et al. [113,128]. However, Eq. (1.2) is somewhat different from the empirical relation of $G=G_\infty(1-a/h)$ [115], where G_∞ is the crystal growth rate for infinite thick films (i.e. bulk) and a is a constant. The empirical relation has been proved to fit experimental results quite well for the film thickness larger than the thickness of lamellae (the relation will not be obeyed when the film thickness is smaller than the lamellar thickness [90,113,128]), though no clear physical meaning has been found [40,113,128].

Other parameters, such as impurity, solvent, thermal history, and substrate, can also affect the growth and selection of instability-resulted morphologies, but none of them has been well studied to date [57,58,77,78]. We finish this section here in a hope of that more future studies will be done to elucidate the fundamental mechanisms of formation and transition of various diffusion-limited growth morphologies, in particular, the role that segment density gradient plays at the growth front.

3. Crystallization kinetics

In previous section we have discussed the morphologies of polymer crystals in thin and ultrathin films. Crystallization kinetics plays the central role in determining intermediate and final morphologies, and all other factors indirectly affect the development and selection of morphology through changing crystallization kinetics. In general, polymer crystallization being one kind of first order phase transitions can be separated into the nucleation step and the subsequent growth step. The nucleation step is called homogeneous nucleation if no preformed nuclei or foreign surfaces are introduced; otherwise it is called heterogeneous nucleation.

Following the nucleation step, nuclei continue to grow by adding new amorphous materials to the existing crystal growth front, resulting in various macroscopic crystal patterns ranging from geometrical-simple single crystals to highly complex superstructures like spherulites. For bulk crystallization, there are several known difficulties in studying the kinetics of both nucleation step and growth step. For example, true homogeneous nucleation may not really be achieved because the foreign particles, which can induce crystallization, are expected to always present in all conventional experiment conditions. And, usually overall crystallization rate is easier to obtain in practical, but existing polymer crystallization theories are originally planned to describe the linear growth of a single lamella. It is possible to obtain the linear growth rate of spherulites through measuring their radius changing with crystallization time. However, according to the morphological characteristics, the formation of spherulites is usually attributed to diffusion-limited growth. Therefore, the radial growth rate is expected to be different from the rate of lamellar growth front. But experimentally it can be fitted to LH theory quite well. Goldenfeld attempted to solve this controversy by extending the well-known Keith–Padden theory [140]. It was proposed that the radial growth rate may be governed by a kinetic term in the equation of diffusion-limited growth, which guarantees the two growth rates, one for

observed spherulites and one for LH theory prediction, agree with each other. Experimental results of linear growth rate of single crystals in bulk state mainly obtained from POM are only available for low molecular weight systems like LMW PEO. As pointed out by Point and Kovacs [141], Putra and Ungar [142], and further by Cheng [7], LH theory alone is insufficient to describe the growth kinetics of single crystals of LMW polymers. As will be presented in the following subsections, crystallization in 2D space is much easier to be followed and may provide some new insight on studying crystallization kinetics.

3.1. Primary nucleation

In practice, homogeneous nucleation can rarely happen in bulk samples due to contamination of foreign particles that lower the nucleation barrier and thus cause heterogeneous nucleation. The traditional approach to observe the elusive homogeneous nucleation is the droplet method, where the droplets are sufficiently small (down to 1 μm) so that most of them will be free for heterogeneous nuclei. At very large supercoolings, the crystal growth rate is much faster than nucleation rate, resulting in a single nucleus crystallizing the whole droplet. This ensures that single nucleation event takes place in one droplet. Taking advantage of this separation of time scales, it is possible to study nucleation independently from crystal growth. In polymer crystallization, a similar approach for studying homogeneous nucleation was recently introduced by Reiter and co-workers who utilized AFM to directly visualize crystallization of PEO in the spherical domains with a radius of 5.9 nm created by microphase separation of a diblock copolymer in thin films on silicon wafers [87,143]. The spherical domains of PEO blocks mimic droplets in traditional approach quite well. The most important result of their direct-space observations is that crystallization occurs randomly across the entire family of spherical domains, and the nucleation events show no correlation between neighboring crystalline sites. The nucleation process characterized by the variation of fraction of crystallized spherical domains with time obeys the common law of $n/n_\infty = 1 - e^{-t/\tau}$ for homogeneous nucleation in the bulk, where n and n_∞ are the number of crystallized spherical domains and the maximum number of crystallizable spherical domains, respectively, and τ is the characteristic time of the process. A large supercooling (60 K) was required to facilitate homogeneous nucleation for domains of PEO blocks in the block copolymer systems studied. In another approach, using dewetted samples, Massa et al. [144] and Massa and Dalnoki-Veress [32] built a new system containing tiny droplets of PEO on a PS substrate to investigate homogeneous nucleation. A smaller supercooling was needed to trigger homogeneous nucleation for this system compared to the block copolymer system (crystallization temperature of -5°C for former and -23°C for later). Moreover, the broad distribution of droplet sizes obtained in dewetted samples allows studying the dependence of the nucleation rate on the length scales. The characteristic time scale τ scales with the size of the droplets R as $\tau \sim R^{-3.2}$. The exponent -3.2 is quite close to -3 , the expected value for homogeneous bulk nucleation, indicating that homogeneous nucleation occurs in the bulk of the droplet rather than on the interface between the bottom of PEO droplets and PS substrate. Further analysis on the dependence of nucleation rate on supercooling adopting data from both dewetted samples and diblock copolymers is consistent with the prediction of the classical nucleation theory, which confirms the homogeneous bulk nucleation in these two very different systems. And it can be concluded that homogeneous bulk nucleation is not affected down to length scales of about 10 nm, an even more remarkable result. These excellent examples of successfully studying homogeneous nucleation are greatly in debt to the simple geometry of quasi-2D space in

thin films which can be directly visualized by optical methods or AFM.

Besides, Lei et al. [68] and Schönherr et al. [38] also claimed that they observed spontaneous homogeneous nucleation during crystallization of relatively thick films (hundreds of nanometers) in the film surface region. The embryos appear and vanish back and forth before they eventually reach a size large enough to grow steadily, which is typical in the context of classical nucleation theory. However, detailed kinetic data were not available, mainly due to too small number of the nucleation event occurring on the film surface.

Usually, spontaneously crystallization of thin films on substrate can be extremely difficult especially for ultrathin films at relatively high crystallization temperatures [20,145,146]. For ultrathin films of PDHS with thickness thinner than 15 nm, there was no detectable crystallinity. Compared with homogeneous nucleation, heterogeneous nucleation possesses much lower nucleation barrier, and thus is widely used to enhance crystallization of polymer thin films. It is often reported that AFM tip can induce nucleation effectively either by nanoindentation [147] or by scratching [27,39,50,51,56]. We studied the effect of both lateral and vertical perturbations from the AFM tip on crystallization of PEO fractions with various molecular weight ranging from 1.0×10^3 to 1.0×10^5 g/mol in thin films on mica substrates. While no crystallization can be induced by lateral perturbations either in hard-tapping or nanoscratch modes in our experiments, tip-induced-nucleation is successfully realized to form flat-on lamella in nanoindentation mode where a vertical tip force is applied to perturb the melt droplets of PEO with molecular weight larger than 1.0×10^4 g/mol. The flat-on orientation of induced crystals implies that the PEO chains are stretched and pack together to form nuclei with chain axis parallel to the tip force direction which is normal to the film surface in nanoindentation mode. Moreover, the tip-induced-crystallization is only possible for high molecular weight, suggesting that the chain length effect, most probably related to the chain entanglement within the melt, is critical for chains to be stretched by the AFM tip. On the other hand, one may expect that if lateral perturbations such as scratching or rubbing on the film surface can lead to crystallization, chains on the film surface should be aligned along the tip moving direction, which is parallel to the film surface, resulting in forming edge-on nuclei which develop into edge-on crystals. Indeed, this has been observed in crystallization of various polymers such as PE ($M_w = 1.2 \times 10^5$ g/mol) [148], PEO ($M_w = 1.0 \times 10^5$ g/mol) [27], PLLA ($M_n = 1.1 \times 10^5$ g/mol) and PDLA ($M_n = 1.2 \times 10^5$ g/mol) [50,51], PCL ($M_n = 1.68 \times 10^5$ and 4.47×10^4 g/mol) [56], and *i*-PS ($M_w = 4.0 \times 10^5$ g/mol) [39]. A general feature of this type of tip-induced crystallization is that the induced edge-on lamellae grow in the direction perpendicular to the tip scratching line, which is quite imaginable since the orientation of the chains within the induced nuclei is parallel to the scratching line and the direction of growth front is determined accordingly. It is also common that these edge-on lamellae will switch into flat-on lamellae after they grow to some extent as described in Section 2.1. Lateral perturbation can even induce nucleation for polymer thin films at glassy state where the deformation of the amorphous sample after scratching or rubbing is expected to be small and limited. Jradi et al. reported that an extremely high nucleation density of edge-on crystals at the edge of the scratched area or within the rubbed region was observed after subsequent isothermal crystallization of *i*-PS at room temperature which is well below its glass temperature [39]. It seems that one can roughly reach a conclusion that AFM tip can induce crystallization as long as chains can be oriented to form stable nuclei and the resulting lamellar orientation depends on direction of the tip force that applied explicitly.

Another way to induce crystallization is self-seeding, which is commonly achieved by heating pre-crystallized samples to some

temperatures near melting temperature followed by holding there for a certain period of time to obtain the number of remaining small crystallites that are needed. Those remaining crystallites act as foreign particles to induce crystallization after quenching the sample to some lower temperature. Self-seeding is an important technique for controlling polymer crystallization in the bulk. For thin film crystallization on solid substrates, one can use it to grow monolayer crystals at low supercooling, which was best demonstrated by Chen and co-workers [29].

3.2. Crystal growth

As compared to primary nucleation, crystal growth in crystallization of polymer thin films has been studied much more intensively. Although direct quantitative comparison of kinetic results obtained from a variety of quite different experimental approaches is hardly possible and controversial cases are occasionally reported, a general trend can be still recognized: there is a systematic deviation of crystallization kinetics from bulk behavior when crystallization takes place in thin films. The rate of crystallization decreases significantly upon reducing film thickness, leading to an increase of crystallization time, a reduction of the linear crystal growth rate and of the Avrami exponent as well. When studying the crystal growth stage, one should always keep in mind that which experimental approach is used and thus which crystal growth rate (overall crystallization rate or linear growth rate) is obtained. Overall crystallization rate usually characterizes the crystallization process using the conversion rate from amorphous materials to crystals, while linear crystal growth rate is obtained by directly measuring the propagation of crystal growth front of individual lamella. For measuring overall crystallization rate, it is difficult to exclude the contribution of nucleation, and moreover, the effects of impingement and non-linear growth arising from diffusion-limited growth are all averaged. In contrast, linear crystal growth rate explicitly relates to the growth process. However, one needs to measure a sufficient number of lamellae that grow under the same conditions, which requires much more experimental effort; sometimes, due to geometrical restrictions of some special samples, it seems impossible to access the linear growth rate experimentally even via imaging techniques.

To date, there are mainly three explanations for interpreting the slowing-down of the crystallization kinetics in thin polymer films: a reduction of molecular mobility due to an increase of the glass transition temperature of the system [27,149], the presence of a reduced mobility layer at the polymer/substrate interface [42–44], and the reduction of the number of active nuclei at a reduction of the thickness [43,150]. The first explanation was proposed by Schönherr et al. who studied the overall crystallization kinetics of PEO ultrathin films using grazing angle RA-FTIR spectroscopy [27]. The FTIR data showed that the half-crystallization times increase considerably when film thicknesses become smaller than ~ 200 nm, an indication for slowing down of the crystallization kinetics. Note that the critical thickness that crystallization kinetics of thin films begins to deviate from the bulk values exceeds the R_g of the polymer by many times, implying that the interactions at polymer/substrate interface may operate over a longer distance than the polymer size as expected. This interacting range coincides well with that of the glass transition temperatures and mobilities of various polymers, leading to the author presuming that the slowing down of the crystallization kinetics is due to the increased glass transition temperature (T_g) of ultrathin PEO films on attractive substrates. It is argued that an increase in T_g is physically reasonable and is well supported by experiments. In particular, an increase in T_g would increase the temperature at which molecular motion ceases (T_∞) and hence slow down the transport of material at the crystal growth front. In fact, the experimental results can be successfully described

by LH theory with a correction of the transport term according to the increase of T_∞ in the linearized Hoffman–Lauritzen equation.

This classical explanation, however, has been challenged recently by Napolitano and Wübberhorst [42,44]. They were aware of the work by Zhang et al. [66,151] in which crystallization kinetics of PET thin films also slowed down with decreasing film thickness but a decrease of the T_g instead of increase was observed, apparently contradicting Schönherr et al.'s results. Moreover, their own results obtained from DS measurements also showed a tremendous slowing down of crystallization kinetics in PHB ultrathin films, while the measured dynamic T_g remains almost constant with the film thickness down to 26 nm. These results mean that the molecular diffusion (characterized by crystallization kinetics) does not necessarily relate to the segmental mobility (characterized by the dynamic T_g), violating the Stokes–Einstein and Debye–Stokes–Einstein relations and generating a paradox. This paradox can be solved, as suggested by Napolitano and Wübberhorst, by invoking the presence of different length scales over which the diffusion and its precursor, the segmental mobility, feel the reduction of film thickness and the interfacial interactions. More particularly, a bilayer model consisting of a reduced mobility layer (RML) and a bulk-like layer has been presented. In the bilayer model, an effective T_g which takes into account of the contributions from both the RML and the bulk-like layer was introduced to replace the dynamic T_g . Since the RML just close to the substrate with an extension in an order of R_g characterized by higher T_g , lower mobility, and almost null expansion coefficient can act first on the static properties (first regime) and then on the dynamical properties (second regime) of the film itself, the effective T_g will exceed the dynamic T_g considerably in the case of attractive substrate at first regime. Consequently, in first regime the crystallization rate will decrease with film thickness when connected to the effective T_g no matter whether the dynamic T_g is the same as or even lower than that of bulk samples. In other words, the reduction of the mobility of the chains at the interface is sufficient to inhibit the transport of material within the entire film resulting in a slowing down of crystallization kinetics, without altering significantly the segmental mobility. The influence of nucleation is considered as a correction factor in bilayer model which further can be simplified by fixing the factor to be 1 and thus lose its thickness dependence, which can be important for slowing down of crystallization kinetics with varying thickness. Here it is worth noting that the bilayer model is quite similar to the three-layer model mentioned previously: both assume a raise of T_g for polymers close to the substrate surface.

The third explanation, as a complement to the second explanation, considers the influence of nucleation. The overall crystallization rate extracted from DS or FTIR was analyzed by a standard approach in terms of the Avrami theory [43,66]. Upon the reduction of film thickness, the Avrami exponent is reduced from 3 to 2 accompanied by an increase of the crystallization time. This implies that either the heterogeneous nucleation is not altered when the dimensionality of the crystallization process decreases with film thickness, or, alternatively, the number of active nuclei that affect the conversion rate of the amorphous phase is reduced by decreasing film thickness. The latter has been predicted by a model by Schultz with an assumption that both the ensemble of crystals nucleated outside of the considered region and the portion of crystals not contained within the borders cannot contribute to the crystallization rate [150]. The model predicts reductions of both crystallization rate and the Avrami exponent, consistent with experiments. However, slowing down of crystallization kinetics without changing Avrami exponent (both 3 for bulk and thin films) has also been reported, indicating that the crystallization proceeds under thermal condition (homogeneous nucleation) [27,149].

The above discussions mainly focus on the deviation of crystallization kinetics of thin films from the bulk without concerning

the exact relation between the crystallization rate and the film thickness. The linear growth rate, which has been mentioned in Section 2.2, depends on film thickness in a form of $1 - a/h$, as first proposed by Sawamura et al. [115] followed by Taguchi et al. [40,113,128] and Grozev et al. [90]. In isothermal crystallization of ultrathin PEO films, a much stronger dependence of the growth rate depression for either linear growth rate or overall crystallization rate with film thickness was obtained [27,149]. The experimental data could be fitted by an exponential dependence in the form of $\exp(1 - a/h)$. These two relations are both empirical without clear physical meaning. By mapping the crystal growth in polymer thin films to DLA growth with finite gas density, we consider that a third relation with the form of h^n is also a candidate to describe the film thickness dependence of crystallization rate as proposed in Section 2.2. Surprisingly, a more complicated relation found in experiments was also reported by Massa et al. who identified a non-monotonic decrease of crystallization rate of PEO thin films upon reducing film thickness [114].

For temperature dependence of crystallization kinetics in thin polymer films, the same laws as that in the bulk are obeyed. Schönherr et al. showed that the linear growth rates of PEO can be successfully described by the LH theory [149]. The effect of the confinement and the interactions at polymer/substrate interface merely cause a constant shift of the linearized Hoffman–Lauritzen plots, keeping the slope of the line unaffected. This shift is attributed to a corrected transport term accounting for the increase of the effective T_g in the LH theory. Li and co-workers studied the cold crystallization of BA-C8 samples using AFM to visualize the growth of single edge-on lamellae [152]. The results show two crystallization regimes (regime I and II) for LMW samples and three crystallization regimes (I, II, and III) for HMW samples, in good agreement with the predictions of the LH theory. They also analyzed the effect of molecular weight on linear growth rates. The crystallization at temperatures near T_g demonstrates a power law of $G \propto M_n^\alpha$, where G is the linear growth rate and M_n is the molecular weight. The exponent α was quite similar for different crystallization temperatures.

When dealing with either the overall crystallization kinetics detected by spatial averaging techniques like DS or FTIR or the growth kinetics determined directly by measuring the size of individual lamella with imaging techniques such as OM or AFM, people might always intend to assume a linear behavior, without concerning the exact nature of the morphology for the growing lamellar crystals. In fact, lamellar morphology should give some hints on the growth mechanism. According to the discussions in Section 2.2, we know that the perfect faceted manner of the growing crystals should point to the nucleation limited growth mechanism, while the more irregular morphologies such as DBM and dendrites are resulted from the diffusion-limited growth. Generally, crystallization proceeds in three sequential steps: (1) units to be crystallized are transported to the crystal growth front (diffusion process); (2) they are incorporated into the crystal lattice at the surface via molecular attachment and detachment usually associated with an activation energy (surface kinetics); and (3) heat is released which should be transported away from the growth front (heat conduction) [122]. If all these steps are fast enough, ideal growth laws can be realized, leading to the equilibrium shape corresponding to the Wulff plot. But in practical, the crystal growth is often governed by the slowest steps and the deviation of both morphology and growth rate from the case of ideal growth is expected. In melt crystallization of polymer thin films, step (3) is always faster than the other two steps and will not be considered further. If step (1) is slow, the crystallization is diffusion-limited (DL); otherwise the crystallization is nucleation limited (NL). It is important to distinguish DL and NL in crystallization because different growth laws of crystal size are obeyed for these two mechanisms. Namely, the lateral crystal

size (R) increases linearly with time (t) in NL growth, while it varies as $R \propto t^{0.5}$ in DL growth if the crystal grows in rounded shape. In the latter case, the crystal cannot grow steadily since the growth rate will eventually vanish when the crystal size approaches infinite, as can be seen from the rate equation: $G \propto t^{-0.5}$. Therefore, to grow large crystals in DL mode, the instabilities of the diffusion field at the growth front should be introduced, which is also responsible for the morphological instabilities. Then, a new growth law may be invoked for this kind of DL growth.

In principle, it is possible to observe all kinds of crystal growth mode by following the development of single lamella in situ. However, the study involving analysis of both NL and DL mechanisms is rarely reported. Recently, using LMW PEO ultrathin film on mica surfaces as a model system, we studied the NL and DL mechanisms and the transition from NL to DL by increasing supercooling [29]. Two PEO fractions, one with both chain ends of $-\text{OH}$ (HPEO, $M_n = 4250$ g/mol) and the other with one $-\text{OCH}_3$ and one $-\text{OH}$ end groups (MHPEO, $M_n = 4700$ g/mol), were crystallized at various supercoolings ($\Delta T = T_m - T_c$). Since the high energy barrier arising from small supercooling and 1D confinement inhibits spontaneous nucleation from the ultrathin films, the self-seeding technique was applied to produce monolayer crystals. The subsequent growth of monolayer crystals was in situ monitored by a tapping-mode AFM coupled with a hot stage.

For MHPEO crystallized at 62°C ($\Delta T = 2.5^\circ\text{C}$), the surface kinetics at the growth front are expected to be very slow and becomes the controlling step since the driving force for crystallization is so small. Fig. 12ax shows an AFM height image captured at a late stage

where the perfect faceted extended chain [IF(0)] single crystals are observed. During crystallization, the single crystals keep their regularly hexagonal shape bounded by two (1 0 0) and four (1 2 0) faces. The distance between two (1 0 0) faces (denoted as $2r$ indexed in Fig. 12a) was measured for a number of sequential recorded images. The plot of r versus t presented in Fig. 12b gives rise to two linear relationships with different slopes, indicating two linear growth rates. These two rates correspond to two growth stages: one for the crystal growing inside the melt droplet containing a self-seed, and the other for the crystal growing from the surrounded wetting layer after the melt droplet was completely transformed into the crystal. The observations of a crystallographically faceted single-crystal shape and the linear growth rate of characteristic crystal size allow one to conclude that the crystal growth under this small supercooling follows the NL mechanism. In contrast to previously reported results of thin film crystallization, the depletion zone was not observed, consistent with NL growth where the transport of material is fast enough to avoid depleting materials near the growth front.

Next, when increase ΔT to 4.5°C , the growing shape of MHPEO single crystal is greatly altered from hexagonal to round rectangular, as can be seen from Fig. 12c compared with Fig. 12a. The characteristic crystal size $2r$, in terms of the distance of two straight (1 0 0) faces as indexed in Fig. 12c, was also measured as a function of crystallization time. The plot of r and the calculated growth rates G as functions of t are given in Fig. 12d. The crystal size grows no longer in linear manner but non-linearly with time. To obtain the explicit dependence of r with t , the G - t curve is fitted to a power

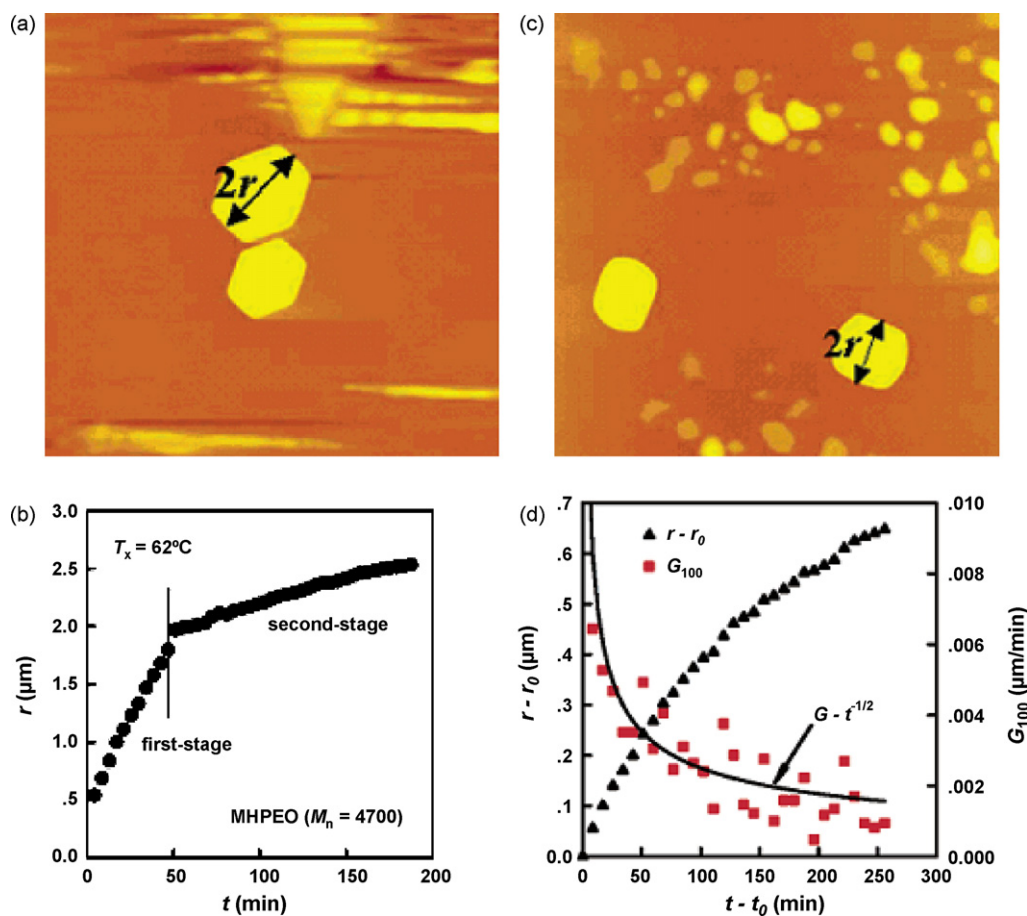


Fig. 12. The AFM height images for MHPEO crystallized at 62°C (a) and 60°C , and their corresponding growth kinetics in terms of half distance between two well-defined crystalline planes. The constant t_0 in (d) is 21.5 min at which the (1 0 0) faces can be recognized and r_0 is the corresponding crystal size at t_0 . The growth rate G was calculated by $\Delta r/\Delta t$ at time t . The solid line represents the theoretical prediction of $G \propto t^{-0.5}$ for DL growth. Figures are reproduced from ref. [29], with permission of the copyright holders.

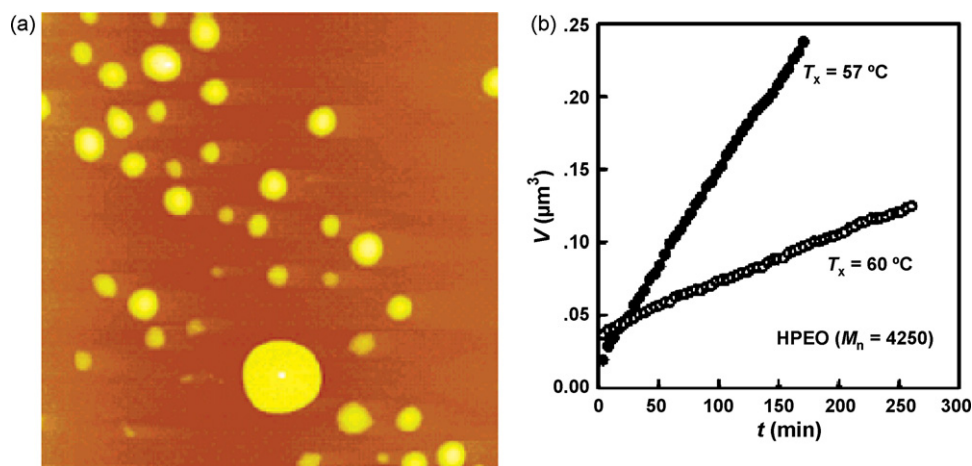


Fig. 13. (a) AFM height image for the HPEO crystallized at 57°C for 166.4 min. (b) The size (V) of HPEO crystals growing at T_x of 57°C and 60°C vs. time (t). Figures are reproduced from ref. [29], with permission of the copyright holders.

law corresponding to DL mechanism. Fig. 12d clearly illustrates that the tendency of G decaying with t follows $G \propto t^{-0.5}$, implying that DL mechanism was invoked in this case. Surprisingly, a slight increase of supercooling from 2.5°C to 4.5°C can lead to the growth mechanism change from NL to DL. Such a small change of temperature can significantly reduce the surface nucleation barrier which strongly depends on ΔT without altering the diffusion process in the temperature range close to T_m . Consequently, the surface kinetics becomes faster than the diffusion step under $\Delta T = 4.5^\circ\text{C}$.

For crystallization of the HPEO we studied, only DL mechanism has been observed for ΔT ranging from 2 to 6°C . Information confirming the DL mechanism are shown in Fig. 13. First, the shape of growing crystals at $\Delta T = 5^\circ\text{C}$ ($T_c = 57^\circ\text{C}$) is almost round without any straight faces (see Fig. 13a). Second, the crystal volume increases linearly with crystallization time (see Fig. 13b). The difference of slopes between 57°C and 60°C shown in Fig. 13b is attributed to higher crystallization driving force at larger ΔT which leads to fast consumption of the HPEO molecules at the growth front. Since IF(0) crystals possess uniform thicknesses, the relation of $V \propto t$ is equivalent to $r \propto t^{0.5}$ in terms of the average lateral growth size r . Third, an obvious depletion zone has been identified near the growth front (data not shown here). All above results ensure the DL mechanism in crystallization of HPEO on mica surface. Compared with the MHPEO with one end group of $-\text{OH}$ and another hydrophobic end group of $-\text{OCH}_3$, the HPEO possesses two $-\text{OH}$ end groups which can interact with the hydrophilic mica surface more strongly. We assume that this end group effect leads the HPEO chains to move slowly within the liquid monolayer. Conse-

quently, the HPEO crystallization on the mica surface just follows the DL mechanism. But for the MHPEO chains with relatively high mobility on the mica surface, increase of the surface nucleation rate with lowering temperature can switch the growth mechanism from NL to DL.

Our observation provides the first experimental evidence for polymer crystallization in thin films which follows the DL mechanism before any morphological instability presents on a micrometer scale. Despite the difference in morphology, both DL processes (with or without morphological instability) are assumed to arise from a concentration gradient of materials to be crystallized, which is related to the depletion zone at the crystal growth front. Fig. 14a illustrates schematically a possible picture that the depletion zone may look like. Instead of assuming that the substrate is continuously covered by polymers and the local thicknesses are different in the depletion zone, we speculate that the wetting layer in the depletion zone may even not be continuous but the PEO molecules within the zone may form a “2D solution” which was already mentioned in Section 2.2, on the basis of the fact that the thickness of the wetting layer being about 4.5 nm is even smaller than the diameter of the unperturbed random coil which is about 5 nm for both HPEO and MHPEO. Then, the surface concentration of PEO molecules (C_s), defined as the number of chains (or monomers) per unit area on the mica surface, can be introduced to describe the diffusion field. This diffusion field, as expected, has lowest concentration at the growth front and the concentration gradually increases until it approaches the normal value of the wetting layer (see Fig. 14b). With this treatment, the mapping from complicated

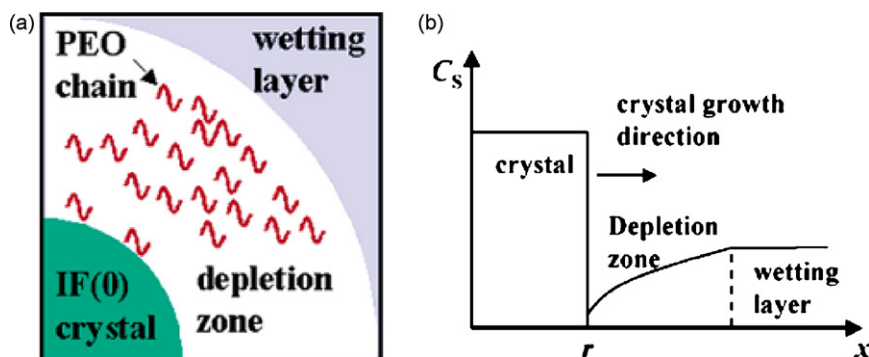


Fig. 14. A schematic showing of the depletion zone between the PEO crystal growth front and the wetting layer (a) and assumed plot of the surface concentration of the PEO molecules C_s as a function of the distance x along the radial direction from the crystal center (b). Figures are reproduced from ref. [29], with permission of the copyright holders.

polymer crystallization on substrate to classical 2D crystal growth has been formulated. We hope this mapping provide some new insights on the study of polymer crystallization in thin films even for DL growth with morphological instabilities. As a first attempt, we have utilized this mapping to discuss the film thickness dependence of the growth rate in the last part of Section 2.2.

With increasing supercooling, the morphological instability will eventually set in and this phenomenon is actually most observed in the literature. It is well established that the tip of the irregular shape can grow steadily with a constant rate, while the rate of change of the number of crystallized units is a size-dependent quantity in the case of DL growth. This kind of growth is strongly related to the morphology, as we have discussed in detailed in Section 2.2. Here, we only make a brief comment. For NL growth and DL growth without morphological instability, the crystal volume V (or crystal mass, the number of crystallized units, etc.) varies with r in the form of $V \propto Ar^2$, where A is a constant related to the shape of the growing crystal. Therefore, the growth rate in terms of V should scale as t^2 for NL growth ($r \propto t$) and t^1 for DL growth without morphological instability ($r \propto t^{1/2}$). For DL growth with morphological instability, however, V relates to r in the form of $V \propto r^{D_f}$ (for 2D case, $1 < D_f < 2$). Then the growth rate in terms of V depends on t in the form of t^{D_f-1} since $r \propto t$, in which the exponent is neither 1 nor 0.5. For example, in DLA growth, the exponent is 0.71 because $D_f = 1.71$. Note that this relation is only valid for true fractal structures because the crystal density $n(r) \propto V/r^2 = r^{D_f-2}$ asymptotically approaches to zero as $r \rightarrow \infty$. In reality, the crystal density should saturate to the amorphous density near the growth front.

4. Metastability of monolayer lamellae

4.1. Thickening behavior

Another very important and intriguing phenomenon in crystallization of polymers is the thickening of polymer crystals after their formation. As was pointed out in the introduction section, lamellae as the most basic form of polymer crystals are non-equilibrium objects trapped in metastable states whose metastability is mainly characterized by lamellar thickness or equivalently the number of folds per molecule. Therefore, from a thermodynamic point of view, there should be an intrinsic tendency for the thinner lamellae relaxing to more stable forms, i.e. thicker lamellae with larger stem length by reducing the number of folds per molecule. This kind of thickening can be triggered by varying thermodynamic parameters like temperature and pressure. Indeed, the thickening of lamellar crystals was discovered in the early days in a study of annealing experiments on PE in bulk using small-angle X-ray scattering (SAXS) to measure long periods which characterize the lamellar thickness [153,154]. Later on, lamellar crystals of a variety of polymers were found able to thicken upon annealing [155]. Early observations of lamellar thickening in bulk crystallization have revealed that the measured long periods of the bulk sample increase when crystallized sample is annealed. Moreover, real space techniques (TEM and POM) show that lamellar thickening is always accompanied by morphological changes. In most cases of early studies, holes are observed to develop in monolayer lamellae; sometimes thickening without the hole-formation is also possible, particularly in lamellar stacks where chains can penetrate into neighboring lamellae.

However, experimental results obtained in the early days either lack real space information or lack of real-time and size information. Now, taking advantages of recently invented AFM and the simpler geometry of thin film systems, one can study the thickening phenomenon of monolayer lamellae down to nanometer scale both in situ and in real time. To narrow our topic, afterwards only the

thickening behavior of monolayer lamellae with flat-on orientation is discussed. Monolayer lamellae on solid substrates normally with uniform thickness at initial stage can be approximately viewed as 2D structures. Obviously, if no materials are supplied from other sources, mass conservation requires that the area covered by monolayer lamellae will decrease when lamellae thicken themselves. In principle, lamellae can reduce their area during thickening by either creating holes inside and thickening at the edge or shrinking their boundaries and thickening inside. A number of experiments on lamellar thickening on substrate have been done and most observations can be categorized into these two modes.

Thickening phenomena are usually observed through annealing fully crystallized lamellae at temperatures between crystallization temperatures (T_c) and melting temperatures (T_m). Sometimes temperatures below T_c or higher than T_m are also applied in annealing. Annealing behavior of monolayer lamellae formed via solution crystallization [26,48,156,157] or in situ melt crystallization in thin films have been investigated [33,158–161] in various polymer systems. One of the most studied systems is LMW PEO ultrathin films on mica or silicon substrates, mainly because the chemical structure of the sample is simple, the monolayer lamellae are easy to prepare, and abundance studies on the LMW PEO crystallization and thickening behavior in bulk of which the results can be used for comparison. Like the case of crystallization in bulk, LMW PEO fractions crystallize into integral folding chain crystals [IF(n)] with a thickness l_n being a integral fraction of the extended chain length L as $l_n = L/(n+1)$, where n is the number of folds per molecules and is determined by the supercooling. The thickness of LMW PEO IF(n) lamellae increases in a quantized manner during thickening. It means that thickened crystals are still IF(n) crystals but with a smaller n . This stepwise increase of lamellar thickness and the fold number of a certain crystal or a part of lamella can be unambiguously distinguished by AFM. It is well known that the T_m of polymer crystals depends on lamellar thickness obeying Gibbs–Thomson equation due to size effect. The thicker the lamella, the higher the T_m will be. The T_m of IF(n) lamellae is denoted as $T_m(n)$.

Reiter et al. have studied the thickening behavior of monolayer lamellae of LMW PEO upon annealing intensively [2,130,131,161–164]. Monolayer lamellae of a LMW PEO fraction ($M_w = 7600$ g/mol, $L = 49$ nm) were prepared in thin films at 25 °C, well below the $T_m(0)$ (64 °C in bulk), and were then sequentially annealed for 5 min at increasingly higher temperatures. Fig. 15 shows some representative high resolution images and cross sections of crystalline domains. For this system, thickening exclusively occurs at crystal edges to form rims; and the width of rims increases with temperatures. It can be interpreted that molecules at the boundaries with fewer neighbors possess a higher mobility in comparison with that in the interior. Discrete changes of lamellar thickness are observed, corresponding to transitions from initial IF(8) to IF(6), IF(4), and then to IF(2) lamellae with increasing annealing temperatures. The fingers of fractal lamellae first contract and then break up into several crystals. Later on, ripening happens and the size of lamellae becomes larger but the number of lamellae decreases. The product of covered area and lamellar thickness is about constant, indicating that the number of molecules in the observed area is conserved. These observations have been reproduced by Monte Carlo simulations using a simple lattice model [131]. For PS-*b*-PEO lamellae annealed at high temperatures, the thickening at crystal edges is more pronounced, resulting in formation of holes inside the lamellae (see Fig. 16). This rim-hole morphology can be found in various annealing conditions for both block copolymers and homopolymers.

By taking advantage of thickening mainly at boundaries, a self-confined state can be created by surrounding the thin interior region with thicker rims. Owing to the confinement effect, this self-confined structure may melt differently compared with crystals

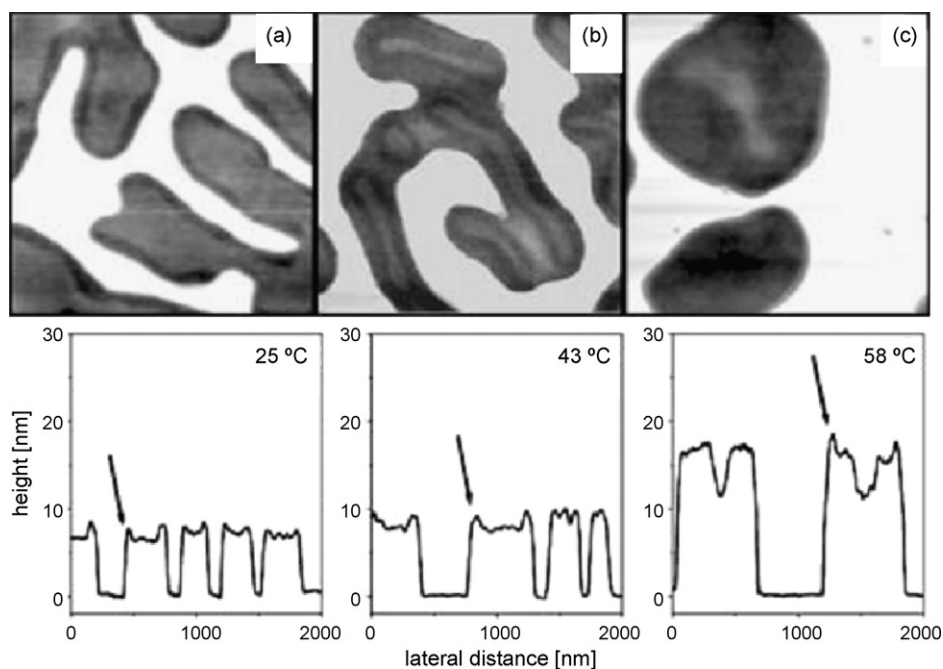


Fig. 15. Typical AFM height images for the thickening of PEO ($M_n = 7600$ g/mol) monolayer crystals. The size of images is $1 \times 1 \mu\text{m}^2$. (a) After crystallization at 25 °C, (b) 5 min/43 °C, (c) 5 min/54 °C. Increasingly darker shades of gray cover a height range from 0 to 50 nm. Typical section profiles corresponding to images (a–c) are shown below. Note the elevation at the edges (marked with arrows) and the changes of the heights at different stages of annealing. Figures are reproduced from ref. [162], with permission of the copyright holders.

of small molecules. Melting starts from surfaces at normal conditions, which typically present the weakest part of crystals of small molecules. In self-confined structures, however, if we anneal them at a temperature between the T_m of inner part and the T_m of rims, the melting will start at the inner part of a crystal, because the rims are stable against this annealing temperature. Moreover, since the inner part is confined, it may become more stable and be difficult to be destroyed, i.e. the superheated phenomenon is expected. Actually, this intriguing phenomenon has been observed in a LMW PEO ($M_n = 4250$ g/mol) system by us [159]. The self-confined structure is successfully prepared by carefully annealing IF(3) lamellae at 35 °C [$T_m(3)$]. After the entire periphery of the IF(3) crystal thickened to IF(2) crystals, this structure is stable at $T_m(3)$ or slight higher temperatures, pointing to a superheated phenomenon. By suddenly bringing the self-confined structure to 39 °C [5 °C lower than the $T_m(2)$], the chains packed in the interior IF(3) crystal unfolds leading to nucleation of holes (see Fig. 17a). More intriguingly, the hole not only can enlarge its size, but also can migrate within the interior part simultaneously. For instance, in Fig. 17a hole A is first nucle-

ated at the beginning of annealing and then “jump” down near the boundary (Fig. 17b) with its size enlarged. Later, hole A explore the right region of the crystal. Note that after the hole moves away, there is always a trace left behind its motion path. The trajectory is in fact a thickened domain with a height of 7–8 nm (see the insets of the height profiles along the dashed lines in Fig. 17d and i) which is less than the height of IF(2) crystal. Thus the trajectory must correspond to a non-integral folding (NIF) state, whose existence can be attributed to the self-confined effect. The thickened trajectory is stable enough to prevent holes pass through it again. Or in other words, holes may possess a self avoiding walk when they travel within the self-confined region. The underlying mechanism still remains unknown.

Most recently, we reported another thickening pathway during annealing, where the thickening occurred mainly in the lamellar interior instead of lateral boundaries [33]. A LMW PEO fraction was also used but with a relatively smaller molecular weight ($M_n = 2000$ g/mol) compared to that used in previous studies, which can only form IF(0) and IF(1) crystals on the substrate. Flat and

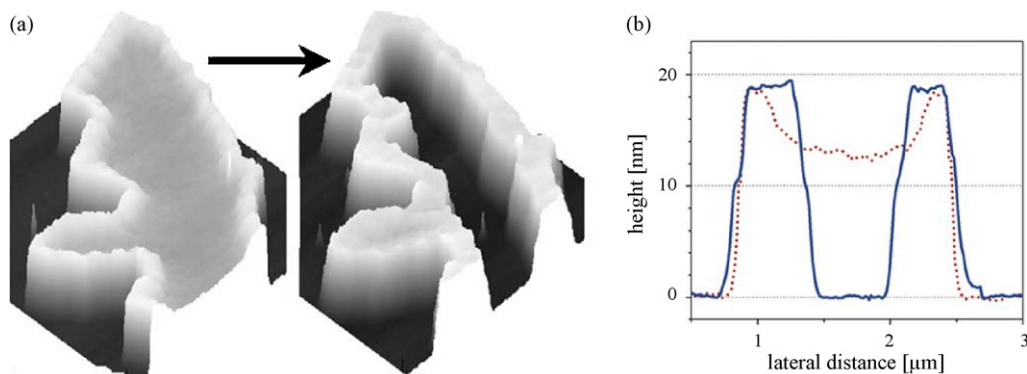


Fig. 16. (a) 3D plots of a monolayer crystal of PS-*b*-PEO ($M_n = 3000$ g/mol for both blocks) crystallized at 45 °C (left) and subsequently annealed for 1 min at 54 °C. (b) Typical section profiles from images in (a). The dotted and the full lines represent the states before and after annealing. Rim-hole structure is clearly demonstrated. Figures are reproduced from ref. [163] with modified labels, with permission of the copyright holders.

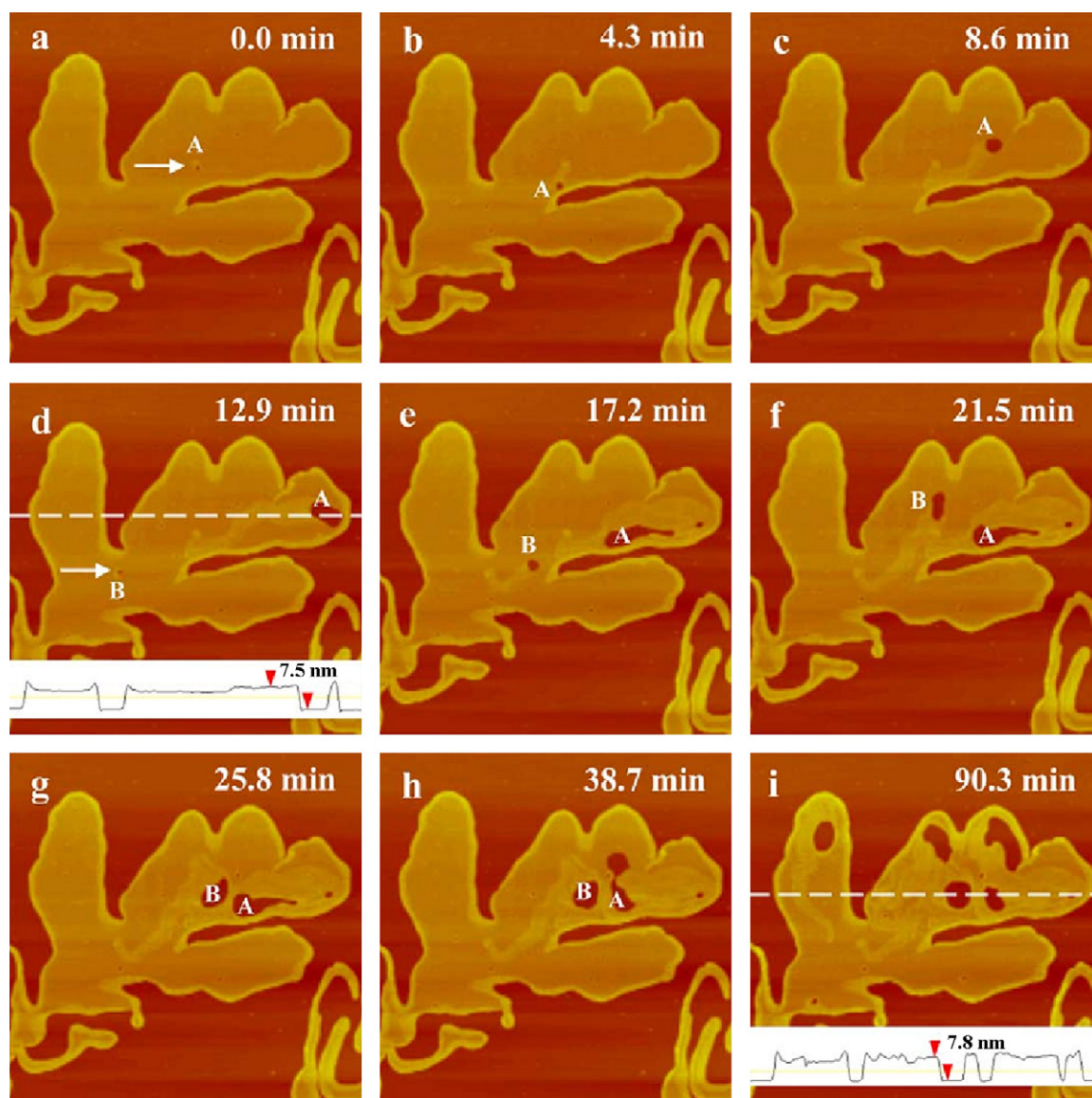


Fig. 17. A set of AFM height images obtained at 39°C for various annealing time. The size of the images is $4.5 \times 4.5 \mu\text{m}^2$. The birthplace of holes A and B are marked with arrows in (a) and (d), respectively. The insets of (d) and (f) are section profiles along the corresponding dashed lines. Figures are reproduced from ref. [159], with permission of the copyright holders.

smooth IF(1) lamellae were prepared via melt crystallization at 18°C or below on freshly cleaved mica. Fig. 18 shows a typical set of AFM height images of IF(1) crystals annealed at 26°C (about 4°C below its melting temperature). As can be seen, the height of

crystal boundary remains unchanged but the total length of crystal boundary decreases significantly. Thickening mainly occurs in the lamellar interior in a way that is similar to nucleation and growth processes. Thickening domains are nearly rounded and their size

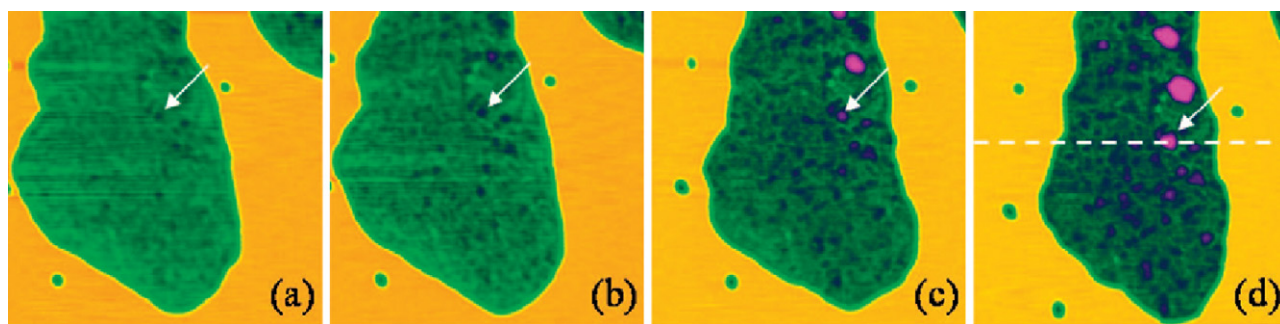


Fig. 18. A set of height images recorded by tapping-mode AFM for the thickening of a PEO monolayer IF(1) crystal annealed at 26°C. The images size is $800 \times 800 \text{nm}^2$ and the annealing times are (a) 7.0, (b) 20.2, (c) 35.9, (d) 50.8 min; the green region is crystal and the orange region is mica surface. Figures are reproduced from ref. [33], with permission of the copyright holders.

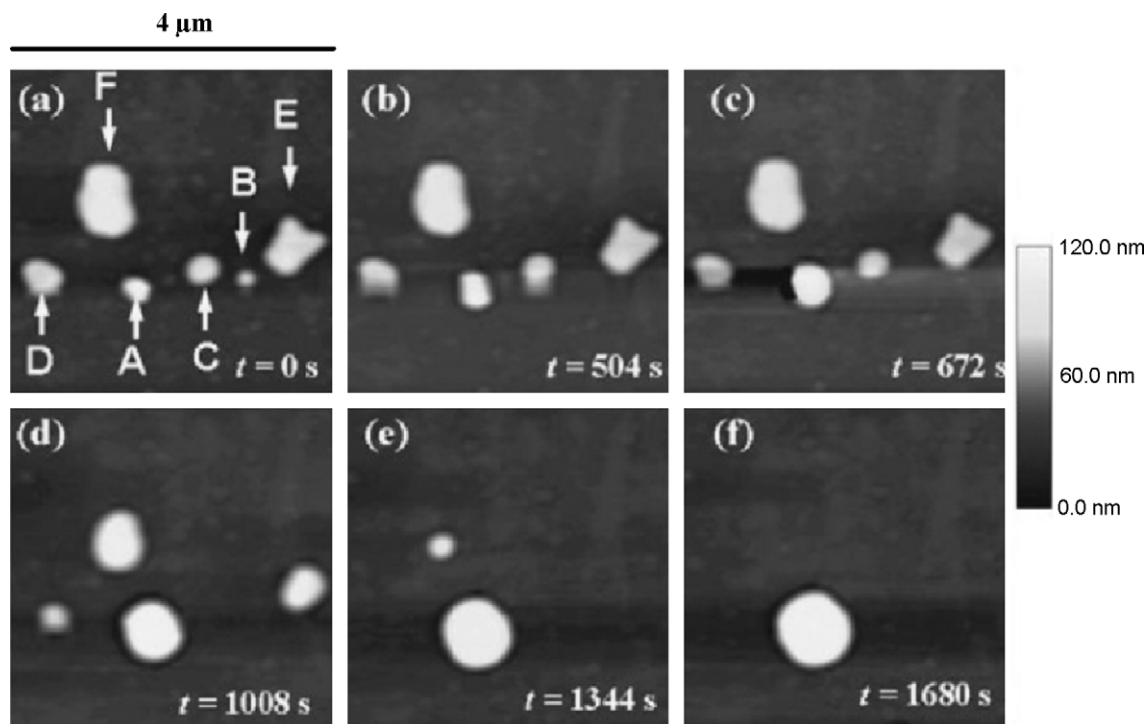


Fig. 19. AFM height images showing thickening of several PEO monolayer crystals annealed at 58 °C. Crystals are marked by characters A to F. Figures are reproduced from ref. [158], with permission of the copyright holders.

grows constantly after they have nucleated. The materials needed for enlarging thickening domains are supplied by shrinking the size of the IF(1) crystal. The possible mechanism for this thickening phenomenon will be discussed in detail in next section. Thickening mainly occurs in the crystal interior during the IF(1)–IF(0) transition [33], while during IF($n+1$)–IF(n) ($n > 2$) transitions thickening almost occurs in the crystal edges [161]. It is interesting to investigate the effect of folding state of lamellar crystals on the thickening behavior. At present, it is not clear whether the thickening pathway shall depend on the folding state.

At late stage, as the thickening proceeds, the original IF crystals will eventually break up into small thickened crystals and then the Ostwald ripening process will set in due to the large surface free energy of many small particles. The system can minimize its energy by eliminating small crystals because they create too many surfaces. As shown in Fig. 19, this process has been clearly demonstrated by Zhai et al. when they annealed IF crystals of a LMW PEO fraction ($M_n = 5000$ g/mol) for a prolonged time at high temperatures [158]. However, the Ostwald ripening in thickening of polymer lamellae is different from common one. Conventional Ostwald ripening occurs as large particles grow and small particles diminish. For Ostwald ripening in thickening of polymer crystals, small but thick crystals can grow by consuming thin crystals, of which the lateral size maybe much larger than that of the growing thick crystals. The fact that this reverse process can happen is because thick crystals are more stable than thin crystals, and this effect overwhelms the increase of surface free energy for small crystals. This is another unique feature of IF crystals.

As thickening phenomena were also reported to occur during isothermal crystallization in bulk [165], one expects to observe lamellar thickening during the thin film crystallization. Basire and Ivanov have detected a slight lamellar thickening (lamellar thickness increases less than 2 nm) upon crystallization of PCL/PVC 75/25 (wt./wt.) blend films [90]. Since the film thickness is ca. 10 μm , this observation must be closer to bulk behavior. Some authors mention that crystal growth front is thinner than fully

grown crystals and lamellar thickening inevitably set in behind the crystal growth front, but no quantitative results have been presented; see chapter 6 in ref. [2] by Hobbs and ref. [53,90]. While in situ observations of lamellar thickening during crystal growth in monolayer lamellae system are not available at present, computer simulations have provided some insights. Sommer and Reiter have simulated polymer crystallization in quasi-2D space using a simplified lattice model [131]. Their simulations predicate that at long time scales the growing crystals will relax to high order structures with larger stem length, leading to morphogenesis similar to that in Figs. 15 and 16. With enhancing the ordering penalty, corresponding to a decrease of temperature in real systems, a typical rim-hole morphology is generated, indicating that the role of crystal edge for relaxation process becomes more pronounced. We expect more pathways that morphological transformations can take during isothermal crystallization as long as T_c is high enough to maintain high chain mobility. In contrast to lamellar thickening of fully crystallized lamellae, the mother phase for thickening may keep growing when reorganization of lamellae proceeds. This may introduce an additional competition effect of growing both original thin lamellae and thickened lamellae, where the thickening proceeds by consuming thin lamellae and the thin lamellae grow by absorbing materials from melt. If it is the case, new reorganized morphologies and especially new kinetics of reorganization process may be realized. The possibility of this type of lamellar thickening and reorganization deserves our special attention.

4.2. Kinetics of monolayer lamellar thickening

Although lamellar thickening are frequently encountered in thin film crystallization, detailed quantitative studies on its kinetics has been reported only very recently. Lamellar thickening and morphogenesis of polymer crystals are much more complicated than the coarsening of small molecule crystals. For small molecule crystals, the coarsening occurs as large crystals grow by consuming smaller crystals due to minimization of interfacial energy by reducing total

perimeters (2D) or surfaces (3D). The coarsening kinetics can be generally described by the Ostwald ripening mechanism. For polymer crystals, however, since folded-chain lamellae correspond to metastable state, a relaxation process first takes place internally to lower free energy. This relaxation can greatly affect the crystal morphologies, leading to thick “dams” and creating holes, as shown in previous section. This process is unnecessary for small molecule crystals since they are already at the final equilibrium crystalline state if the size effect is not taken into account. After or during the relaxation, coarsening of polymer lamellae similar to small molecule crystals may then set in. The late stage coarsening of polymer crystals is still very different from conventional Ostwald ripening: as just mentioned above, the small thick crystals will grow instead of the large thin crystals. Most previous studies, as summarized in the previous section, focused on the morphological evolution when lamellae are annealed, especially on the pattern where the thickening mainly occurs at the boundaries and holes develop inside. As it is hard to precisely measure the height and the area, those experimental results are somewhat less quantified.

For thin film systems, it is important to know the variation of crystal height (thickness) and area (volume) with time and the variation of their growth speeds with annealing temperature, because these quantities can be directly compared with those obtained from annealing experiments in bulk. The SAXS measurements for annealing bulk samples clearly revealed that lamellar thickness increased after the formation of initial lamellar stacks. Two basic observations of lamellar thickening in bulk are: (1) the thickness increases linearly with logarithm of time, and (2) the thickening rate of thickness increase with annealing temperatures. If the mechanism of thickening is not significantly disturbed by 2D confinement, one should expect that the growth mode of thickening is the same for both bulk and 2D cases.

Zhai et al. have obtained the height and area variations of a thickened part within the unthickened crystal of a LMW PEO fraction, both of which show a linear growth at initial stage and a nearly zero growth after a certain annealing time at a temperature of 50 °C [158]. On the basis of this observation, they conclude that at this annealing temperature the thickened part is unable to cause the rest IF(1) crystal to be thickened into IF(0) crystal. However, it is also possible that the growth of thickening part is very slow and their observation time is limited. One complication involved in the experiments by Zhai et al. and others [161] is that the annealing is performed non-isothermally. Thus the effects of annealing time and annealing temperature are strongly coupled together. This hinders one to elucidate the roles of these two factors separately.

In a most recent study, we reported a quantitative analysis of thickening of LMW PEO lamellar crystals on mica surfaces and the thickening was also modeled by a phase field simulation [33]. The morphological evolution during thickening was monitored in situ using AFM which was discussed in previous section (see Fig. 18 and the related text). As thickening domains are mainly generated inside the original crystal of IF(1) monolayer and they are nearly round in shape, we can easily measure their heights and lateral sizes from the section profiles obtained via sectioning the thickening domain along a horizontal line which passes through the point with maximum location. Fig. 20 shows a series of section profiles of the thickening domain indicated by the white arrow in Fig. 18. The peaks at the middle of the profiles represent the thickening domain. Note that the height of the thickening domain (H) is chosen as the maximum height of this domain even though the height across the entire thickening domain is non-uniform. The size of the thickening domain (HW) is the peak width at half height. The measured values of these two quantities as functions of annealing time are shown in the inset of Fig. 20. At the very beginning, no clear-cut interface between thickened domain and mother phase can be

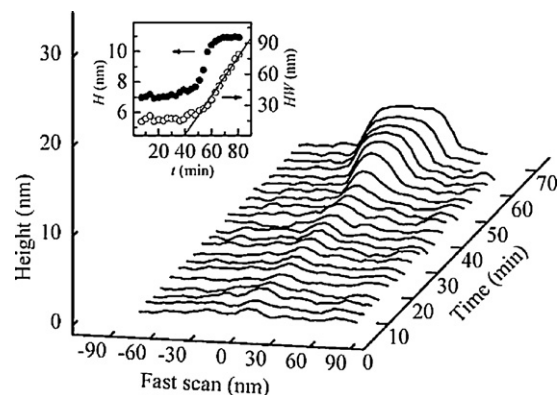


Fig. 20. Section profiles through the centers of a typical thickening domain marked with arrows in Fig. 18. The inset plots the values of the peak value (H) and the half-height peak width (HW) of section profiles as functions of t . Figure reproduced from ref. [33], with permission of the copyright holders.

identified; both H and HW are randomly distributed around their minimum values, with a fluctuation amplitude of ~ 0.7 nm and a fluctuation scale of ~ 15 nm. After an induction period of ~ 20 min, a distinguishable thickened domain emerges: the HW increases linearly and H grows first slowly followed by a rapid approach to the thickness of IF(0) crystal. The increase of H is sigmoidal, which remarkably resembles the long period evolution pattern observed by scattering method for bulk samples. Here only a single domain is measured, while for bulk measurements the thickness of a large number of thickened domains (it is not clear what shape they take and how they distribute in the bulk) are averaged. In addition, the lateral size HW , which is hard to be detected in bulk, is found to grow linearly when H begins to grow rapidly.

As indicated by Figs. 18 and 20, the emerging and growing of the thickening domain are similar to nucleation and growth predicted by the classical nucleation theory (CNT). Actually, a nucleation-type model has been proposed for nearly five decades to interpret experimental observations of thickening in bulk [155,166–168]. The model assumes that a rectangular nucleus with a height of the length of one repeating unit (d_0) is formed on the fold surface. Once the nucleus appears, the thickened domain with its thickness constant fast propagates in the lateral direction to cover the fold surface. The rate of growth of nucleus is so fast that another nucleation event could not occur until the whole lamella is thickened to $l + d_0$, where l is the thickness before thickening. This nucleation-type model can explain the linear logarithm increase of lamellar thickness with annealing time which is observed in thickening of lamellae. The strong time dependence of the rate of thickening on approach to the melting temperature can also be explained by taking into account of partial melting [155] or of introducing an activation energy for sliding diffusion of molecular backbones in the crystal [166,167]. However, the assumption of formation of nucleus and fast growth in lateral direction cannot be observed directly in bulk. In our quasi-2D observations, the nucleation process has been successfully observed. The sigmoidal increase of lamellar thickness may lead to a linear logarithm increase of lamellar thickness with annealing time. But unlike the assumptions of the nucleation-type model, our observations reveal that the lateral growth of thickened domains is not that fast. Therefore, there are other nucleation events after one nucleus is formed, resulting in multiple thickening domains growing simultaneously, which is clearly shown in Fig. 18.

Moreover, we can count the number of thickening domains with increasing annealing time and the variation of the number density ρ_N (number of thickening per area) is calculated accordingly. The results for IF(1) monolayers annealed at various temperatures

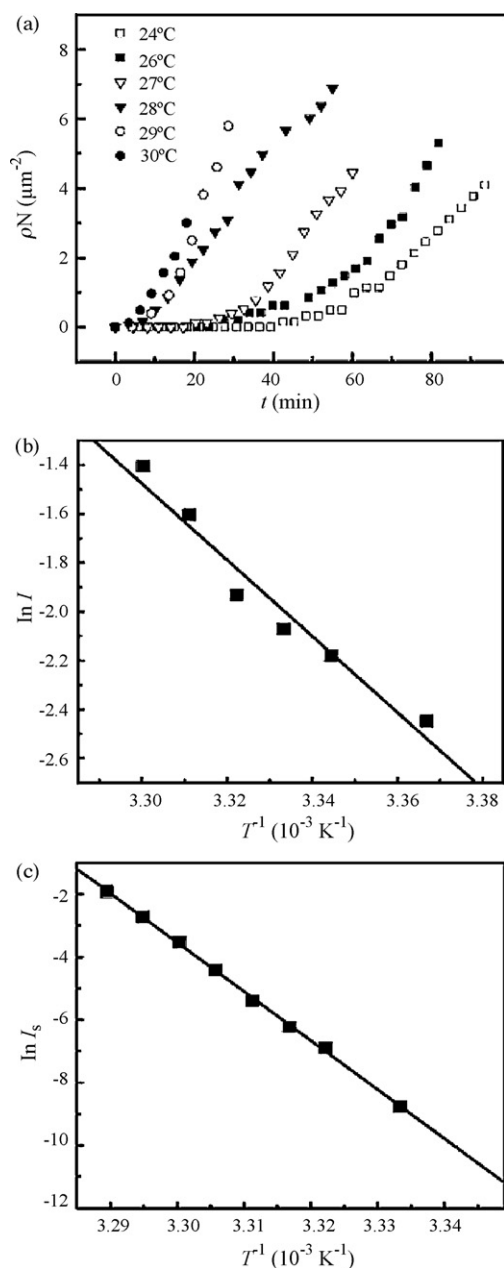


Fig. 21. Evolution of the number density of thickening domains for monolayer crystals (ρ_N) annealed at various T_s (a). T -dependence of nucleation rates measured as the rate of variation of ρ_N at the steady growth stage (b) and counted from simulation (c). Figure reproduced from ref. [33].

(24–30 °C) are illustrated in Fig. 21a. For all ρ_N - t curves, an induction period is followed by a steady linear growth of ρ_N , which is typical for all nucleation phenomena. To obtain the nucleation rate I , one can find the slope of the steady linear growth part using a linear regression technique. Note that the nucleation rate obtained here reflects only the rate of increasing the number density of thickened domains but not the thickening rate usually referred in literature which is the rate of increasing the thickness of thickened domains. The analogue for the latter in our studies can be obtained from differentiating H with t . Upon increasing T , the nucleation rate is enhanced with a sharply drop of induction period. The increase of nucleation rate I with annealing temperature seems to obey the Arrhenius law (see Fig. 21b) with an activation energy of $129.7 \text{ kJ mol}^{-1}$. This dependence is in contrast

to classical nucleation such as polymer crystallization or melting where the logarithm of nucleation rate is proportional to ΔT^{-2} (ΔT is the supercooling or superheating). Therefore, the CNT applied for polymer crystallization or melting is not readily applicable to explain this observation.

For the first preliminary try, we built a model with consideration of the curved interface between thickening domains and mother phase. A mesoscale simulation technique, the so called phase field simulation based on the Ginzburg–Landau theory, was applied to study the transient nucleation phenomenon. Taking advantage of the simplicity of our 2D crystalline system, we are able to construct a free energy functional containing the well-defined physical parameters only. In our model, each stem is coarse-grained into a single point, which can be naturally mapped to the grid point in finite difference scheme which is used in our actual simulations. Each grid point is associated with an order parameter ϕ defined by l/l_0 , where l is the length of the stem in monomer number (the local thickness) and l_0 the contour length of the whole chain. Two kinds of free energy are considered: local and nonlocal. The local free energy consists of the free energy reduction due to crystallization, the excess energies arising from defects created by chain ends buried in crystal lattice and chain folds on top and bottom surfaces, and a deformation energy of chain folds caused by extending or compressing. The nonlocal free energy includes the surface energy of top and bottom surfaces of a crystal monolayer, while the surface free energy of the lateral surfaces is neglected for simplification. The free energy functional is a combination of the local and nonlocal terms.

Phase field simulations (time-dependent Ginzburg–Landau equation type A) are performed on a square lattice for convenience without concerning the curved boundaries of actual observing IF(1) crystals. But in addition to the common phase field equation, a Lagrange multiplier is introduced to ensure mass conservation. We have collected a number of images from numerical simulations that can be directly compared to the experimental observations. As a result, the evolution patterns from simulations agree with experimental results for many aspects, including (1) roughening of the top surface of monolayer, (2) the present of induction period, (3) the curved shape of thickening domains, (4) the sigmoidal growth of H and linear growth of HW , and (5) the evolution of the number density of thickening domains. These coincidences confirm that the phase field simulation is feasible in reproducing experimental observations.

In addition, the T -dependence of nucleation rate was also studied by simulation. In simulation, we find that the nucleation rate is quite sensitive to the property of surface free energy of the top surface σ_e . Keeping σ_e a constant will result in decrease of nucleation rate with T , contrary to the experimental observations. However, if we assume that σ_e can be expressed as $C-BT$, a linear decrease function of T , the Arrhenius-like dependence of nucleation rate with T can be successfully reproduced as shown in Fig. 21c. It can be understood in the line of following arguments. With increasing T , σ_e will become smaller and stems can protrude out of the top surface more easily, yielding a higher possibility for nucleation. In other words, the surface free energy is mapped to the line tension which hinders the nucleation in 2D case. It has become clear that the chain sliding motion provides the manner of thickening whereas the surface free energy decides whether or not the sliding motion can actually lead to the nucleation. Furthermore, if we keep the T and other parameters constant to perform similar simulation, the nucleation rate decreases with increasing σ_e and the nucleation process stops beyond some critical value. This may explain why some folded-chain crystals cannot thicken or only thicken at T rather close to their melting temperatures. The reason is that the surface energy of their fold surface exceeds a critical value corresponding to a particular parameter space.

Our observations and simulations imply that nucleation and growth is also one of possible mechanisms for lamellar thickening in bulk state, but the growth rate is not that fast as those assumed in the nucleation-type model. Thus multinucleation growth mechanism (analogy to regime II in HL theory for polymer crystallization) is more suitable for describing lamellar thickening than mononucleation growth (analogy to regime I in HL theory). One should anticipate that similar results will be obtained from the nucleation-type model using multinucleation growth assumption, though it has not been done yet.

It is clear that 2D geometry provides us a unique way to study lamellar thickening, and moreover, to study the nucleation phenomenon in real space and in situ with the physical picture fully consistent with the CNT. The simulation tells the existence of an energy barrier associated with the size of critical nuclei. With the enough large size of the critical nuclei and 2D geometrical restriction, our monolayer system also allows one to directly observe the nucleation process in the nascent stage, which is only possible for some special systems like colloidal system before this study.

5. Summary

The morphologies, the crystallization kinetics, and the transformation between crystals with various metastabilities are three most important topics in study of polymer crystallization in thin films on solid substrates. However, they are not isolated problems but usually relate to each other. The development of morphologies is controlled by both crystallization kinetics, which are further determined by the interactions between macromolecules and substrates as well as the properties of macromolecules at molecular scale, and the transformation (thickening) of metastable states if present. On the other hand, from the growing pattern of polymer crystals, crystallization kinetics and kinetics of transformation of metastable states can be deduced, which may further help discover underlying mechanisms. As expected, 2D geometry can greatly affect polymer crystallization in many aspects. Sometimes the interactions between polymer and substrate can also be critical, but this effect is much harder to investigate.

The slow growth rates together with the possibility to form simple planar morphologies which can be naturally cast to a 2D problem make polymer crystals on solid substrates ideal model systems for fundamental studies of nucleation, growth, and transformation of such metastable phases. Thus, combining these model experiments with theoretical concepts, including computer simulations, provides a highly promising approach for improving our understanding of polymer crystallization and may also shed some light on central questions of crystal growth phenomenon in general.

Acknowledgements

Acknowledgement is made to the National Natural Science Foundation of China (20025414, 20234020, 20374003, and 20774006). We thank the students and colleagues for valuable discussion during the preparation of the manuscript. We particularly appreciate here all the supporting from the College of Chemistry of Peking University.

References

- [1] G. Reiter, G.R. Strobl, *Progress in Understanding of Polymer Crystallization*, Springer, Berlin Heidelberg, 2007.
- [2] G. Reiter, J.U. Sommer, *Polymer Crystallization: Observations, Concepts and Interpretations*, Springer-Verlag, Berlin Heidelberg, 2003.
- [3] A. Keller, *Philos. Mag.* 2 (1957) 1171.
- [4] P.H. Till, *J. Polym. Sci.* 24 (1957) 301.
- [5] E.W. Fischer, *Naturforsch* 12 (1957) 753.
- [6] R. Jaccodine, *Nature* 176 (1955) 305.
- [7] S.Z.D. Cheng, *Phase Transitions in Polymers: The Role of Metastable States*, Elsevier, Amsterdam, 2008.
- [8] K. Armitstead, G. Goldbeck-Wood, *Adv. Polym. Sci.* 100 (1992) 219.
- [9] J.D. Hoffman, R.L. Miller, *Polymer* 38 (1997) 3151.
- [10] J.D. Hoffman, G.T. Davis, J.I. Lauritzen, in: Hannay (Ed.), *Treatise on Solid State Chemistry*, Plenum Press, New York, 1976.
- [11] J. John, I. Lauritzen, J.D. Hoffman, *J. Chem. Phys.* 31 (1959) 1680.
- [12] D.M. Sadler, G.H. Gilmer, *Phys. Rev. B* 38 (1988) 5684.
- [13] D.M. Sadler, G.H. Gilmer, *Phys. Rev. Lett.* 56 (1986) 2708.
- [14] J. Baert, P. Van Puyvelde, *Macromol. Mater. Eng.* 293 (2008) 255.
- [15] P.D. Olmsted, W.C. Poon, T.C. McLeish, N.J. Terrill, A.J. Ryan, *Phys. Rev. Lett.* 81 (1998) 373.
- [16] G. Matsuba, K. Kaji, K. Nishida, T. Kanaya, M. Imai, *Macromolecules* 32 (1999) 8932.
- [17] G. Strobl, *Prog. Polym. Sci.* 31 (2006) 798.
- [18] G. Strobl, *Eur. Phys. J. E* 18 (2005) 295.
- [19] G. Strobl, *Eur. Phys. J. E* 3 (2000) 165.
- [20] C.W. Frank, V. Rao, M.M. Despotopoulou, R.F.W. Pease, W.D. Hinsberg, R.D. Miller, J.F. Rabolt, *Science* 273 (1996) 912.
- [21] W. Bi, J.S. Teguh, E.K.L. Yeow, *Phys. Rev. Lett.* 102 (2009) 48302.
- [22] A. Toda, M. Okamura, K. Taguchi, M. Hikosaka, H. Kajioka, *Macromolecules* 41 (2008) 2484.
- [23] J.K. Hobbs, *Polymer* 47 (2006) 5566.
- [24] A. Tracz, G. Ungar, *Macromolecules* 38 (2005) 4962.
- [25] Y. Wang, M. Rafailovich, J. Sokolov, D. Gersappe, T. Araki, Y. Zou, A.D.L. Kilcoyne, H. Ade, G. Marom, A. Lustiger, *Phys. Rev. Lett.* 96 (2006) 28303.
- [26] S.N. Magonov, N.A. Yerina, G. Ungar, D.H. Reneker, D.A. Ivanov, *Macromolecules* 36 (2003) 5637.
- [27] H. Schönherr, C.W. Frank, *Macromolecules* 36 (2003) 1188.
- [28] G. Reiter, J.U. Sommer, *Phys. Rev. Lett.* 80 (1998) 3771.
- [29] D.S. Zhu, Y.X. Liu, E.Q. Chen, M. Li, C. Chen, Y.H. Sun, A.C. Shi, R.M. VanHorn, S.Z.D. Cheng, *Macromolecules* 40 (2007) 1570.
- [30] X. Zhai, W. Wang, G. Zhang, B. He, *Macromolecules* 39 (2006) 324.
- [31] M. Wang, H. Braun, E. Meyer, *Macromol. Rapid Comm.* 23 (2002) 853.
- [32] M.V. Massa, K. Dalnoki-Veress, *Phys. Rev. Lett.* 92 (2004) 255509.
- [33] Y.X. Liu, J.F. Li, D.S. Zhu, E.Q. Chen, H.D. Zhang, *Macromolecules* 42 (2009) 2886.
- [34] Z. Hu, F. Zhang, B. Du, H. Huang, T. He, *Langmuir* 19 (2003) 9013.
- [35] L. Kailas, C. Vasilev, J. Audinot, H. Migeon, J.K. Hobbs, *Macromolecules* 40 (2007) 7223.
- [36] M. Franke, N. Rehse, *Macromolecules* 41 (2008) 163.
- [37] X. Wang, W. Hou, J. Zhou, L. Li, Y. Li, C. Chan, *Colloid Polym. Sci.* 285 (2007) 449.
- [38] H. Schönherr, R.M. Waymouth, C.W. Frank, *Macromolecules* 36 (2003) 2412.
- [39] K. Jradi, S. Bistac, M. Schmitt, A. Schmatulla, G. Reiter, *Eur. Phys. J. E* 29 (2009) 383.
- [40] K. Taguchi, H. Miyaji, K. Izumi, A. Hoshino, Y. Miyamoto, R. Kokawa, *Polymer* 42 (2001) 7443.
- [41] K.L. Beers, J.F. Douglas, E.J. Amis, A. Karim, *Langmuir* 19 (2003) 3935.
- [42] S. Napolitano, M. Wübbenhorst, *J. Phys. Chem. B* 111 (2007) 5775.
- [43] S. Napolitano, M. Wübbenhorst, *J. Phys. Conds. Matter.* 19 (2007) 205121.
- [44] S. Napolitano, M. Wübbenhorst, *Macromolecules* 39 (2006) 5967.
- [45] M.J. Capitán, D.R. Rueda, T.A. Ezquerro, *Macromolecules* 37 (2004) 5653.
- [46] A. Frösrdorf, E.M. Woo, L. Lee, Y. Chen, S. Förster, *Macromol. Rapid Comm.* 29 (2008) 1322.
- [47] K. Kawashima, R. Kawano, T. Miyagi, S. Umemoto, N. Okui, *J. Macromol. Sci. B* 42 (2003) 889.
- [48] X. Wang, J. Zhou, L. Li, C. Chan, *Macromol. Rapid Comm.* 28 (2007) 2001.
- [49] H. Li, W. Nie, C. Deng, X. Chen, X. Ji, *Eur. Polym. J.* 45 (2009) 123.
- [50] D. Maillard, R.E. Prud'homme, *Macromolecules* 41 (2008) 1705.
- [51] D. Maillard, R.E. Prud'homme, *Macromolecules* 39 (2006) 4272.
- [52] Y. Yuryev, P. Wood-Adams, M. Heuzey, C. Dubois, J. Brisson, *Polymer* 49 (2008) 2306.
- [53] Y. Kikkawa, H. Abe, M. Fujita, T. Iwata, Y. Inoue, Y. Doi, *Macromol. Chem. Phys.* 204 (2003) 1822.
- [54] Y. Kikkawa, H. Abe, T. Iwata, Y. Inoue, Y. Doi, *Biomacromolecules* 2 (2001) 940.
- [55] B.C. Okerberg, B.C. Berry, T.R. Garvey, J.F. Douglas, A. Karim, C.L. Soles, *Soft Matter* 5 (2009) 562.
- [56] M. Fujita, Y. Takikawa, H. Sakuma, S. Teramachi, Y. Kikkawa, Y. Doi, *Macromol. Chem. Phys.* 208 (2007) 1862.
- [57] V.H. Mareau, R.E. Prud'homme, *Macromolecules* 38 (2005) 398.
- [58] V.H. Mareau, R.E. Prud'homme, *Polymer* 46 (2005) 7255.
- [59] A. Toda, I. Kojima, M. Hikosaka, *Macromolecules* 41 (2008) 120.
- [60] J.Y. Kim, M.H. Kwon, Y.K. Min, S. Kwon, D.W. Ihm, *Adv. Mater.* 19 (2007) 3501.
- [61] Y. Zhang, S. Mukoyama, Y. Hu, C. Yan, Y. Ozaki, I. Takahashi, *Macromolecules* 40 (2007) 4009.
- [62] Y. Zhang, S. Mukoyama, K. Mori, D. Shen, S. Yan, Y. Ozaki, I. Takahashi, *Surf. Sci.* 600 (2006) 1559.
- [63] Y. Liang, M. Zheng, K.H. Park, H.S. Lee, *Polymer* 49 (2008) 1961.
- [64] Y. Sakai, M. Imai, K. Kaji, M. Tsuji, *J. Cryst. Growth* 203 (1999) 244.
- [65] Y. Sakai, M. Imai, K. Kaji, M. Tsuji, *Macromolecules* 29 (1996) 8830.
- [66] Y. Zhang, Y. Lu, Y. Duan, J. Zhang, S. Yan, D. Shen, *J. Polym. Sci. B* 42 (2004) 4440.
- [67] D.A. Ivanov, G. Bar, M. Dosière, M.H.J. Koch, *Macromolecules* 41 (2008) 9224.
- [68] Y. Lei, C. Chan, J. Li, K. Ng, Y. Wang, Y. Jiang, L. Li, *Macromolecules* 35 (2002) 6751.

- [69] C. Chan, L. Li, *Adv. Polym. Sci.* 188 (2005) 1.
- [70] L. Li, C. Chan, K.L. Yeung, J. Li, K. Ng, Y. Lei, *Macromolecules* 34 (2001) 316.
- [71] L. Li, C. Chan, J. Li, K. Ng, K. Yeung, L. Weng, *Macromolecules* 32 (1999) 8240.
- [72] F. Xia, B. Razavi, H. Xu, Z.Y. Cheng, Q.M. Zhang, *J. Appl. Phys.* 92 (2002) 3111.
- [73] Y. Wang, S. Ge, M. Rafailovich, J. Sokolov, Y. Zou, H. Ade, J. Lüning, A. Lustiger, G. Maron, *Macromolecules* 37 (2004) 3319.
- [74] C. Basire, D.A. Ivanov, *Phys. Rev. Lett.* 85 (2000) 5587.
- [75] V. Ferreiro, J.F. Douglas, J.A. Warren, A. Karim, *Phys. Rev. E* 65 (2002) 51606.
- [76] V. Ferreiro, J.F. Douglas, J.A. Warren, A. Karim, *Phys. Rev. E* 65 (2002) 42802.
- [77] B.C. Okerberg, H. Marand, J.F. Douglas, *Polymer* 49 (2008) 579.
- [78] B. Okerberg, H. Marand, *J. Mater. Sci.* 42 (2007) 4521.
- [79] M. Wang, H. Braun, E. Meyer, *Macromolecules* 37 (2004) 437.
- [80] M. Wang, H. Braun, E. Meyer, *Polymer* 44 (2003) 5015.
- [81] I. Volegova, A. Buzin, *Polym. Sci. Ser. A* 49 (2007) 1014.
- [82] P. Yang, Y. Han, *Langmuir* 25 (2009) 9960.
- [83] G. Reiter, L. Vidal, *Eur. Phys. J. E* 12 (2003) 497.
- [84] J. Fu, Y. Wei, L. Xue, B. Luan, C. Pan, B. Li, Y. Han, *Polymer* 50 (2009) 1588.
- [85] Y. Wei, C. Pan, B. Li, Y. Han, *J. Chem. Phys.* 126 (2007) 104902.
- [86] J. Sun, Z. Hong, L. Yang, Z. Tang, X. Chen, X. Jing, *Polymer* 45 (2004) 5969.
- [87] G. Reiter, G. Castelein, J.U. Sommer, A. Röttele, T. Thurn-Albrecht, *Phys. Rev. Lett.* 87 (2001) 226101.
- [88] G. Reiter, G. Castelein, P. Hoerner, G. Riess, J.U. Sommer, G. Floudas, *Eur. Phys. J. E* 2 (2000) 319.
- [89] G. Reiter, G. Castelein, P. Hoerner, G. Riess, A. Blumen, J.U. Sommer, *Phys. Rev. Lett.* 83 (1999) 3844.
- [90] N. Grozev, I. Botiz, G. Reiter, *Eur. Phys. J. E* 27 (2008) 63.
- [91] J.K. Hobbs, R.A. Register, *Macromolecules* 39 (2006) 703.
- [92] Y. Zheng, M.L. Bruening, G.L. Baker, *Macromolecules* 40 (2007) 8212.
- [93] Y. Ma, W.B. Hu, G. Reiter, *Macromolecules* 39 (2006) 5159.
- [94] P. Bernazzani, R. Sanchez, *Eur. Phys. J. E* 26 (2008) 427.
- [95] A. Keller, G. Goldbeck-Wood, in: Aggarwal, Russo (Eds.), *Comprehensive Polymer Science: 2nd Supplement*, Elsevier, Oxford, 1996, p. 241.
- [96] G. Ungar, X. Zeng, *Chem. Rev.* 101 (2001) 4157.
- [97] Y. Takenaka, H. Miyaji, A. Hoshino, A. Tracz, J.K. Jeszka, I. Kucinska, *Macromolecules* 37 (2004) 9667.
- [98] J. Fu, S.G. Urquhart, *Langmuir* 23 (2007) 2615.
- [99] Y. Jiang, D. Yan, X. Gao, C.C. Han, X. Jin, L. Li, Y. Wang, C. Chan, *Macromolecules* 36 (2003) 3652.
- [100] H.G. Haubruge, R. Daussin, A.M. Jonas, R. Legras, *Polymer* 44 (2003) 8053.
- [101] D.A. Ivanov, Z. Amalou, S.N. Magonov, *Macromolecules* 34 (2001) 8944.
- [102] C. Qiao, J. Zhao, S. Jiang, X. Ji, L. An, B. Jiang, *J. Polym. Sci. B* 43 (2005) 1303.
- [103] Y. Jiang, X. Jin, C.C. Han, L. Li, Y. Wang, C. Chan, *Langmuir* 19 (2003) 8010.
- [104] Y. Lei, C. Chan, Y. Wang, K. Ng, Y. Jiang, L. Lin, *Polymer* 44 (2003) 4673.
- [105] J. Zhou, L. Li, J. Lu, *Polymer* 47 (2006) 261.
- [106] J. Zhou, J. Liu, S. Yan, J. Dong, L. Li, C. Chan, J.M. Schultz, *Polymer* 46 (2005) 4077.
- [107] Z. Hu, H. Huang, F. Zhang, B. Du, T. He, *Langmuir* 20 (2004) 3271.
- [108] Y.K. Godovsky, S.N. Magonov, *Langmuir* 16 (2000) 3549.
- [109] A. Tracz, I. Kucinska, J.K. Jeszka, *Polymer* 47 (2006) 7251.
- [110] E. Meyer, H. Braun, *J. Phys. Conds. Matter* 17 (2005) S623.
- [111] Z. Ma, G. Zhang, X. Zhai, L. Jin, X. Tang, M. Yang, P. Zheng, W. Wang, *Polymer* 49 (2008) 1629.
- [112] G. Zhang, L. Jin, Z. Ma, X. Zhai, M. Yang, P. Zheng, W. Wang, G. Wegner, *J. Chem. Phys.* 129 (2008) 224706.
- [113] K. Taguchi, A. Toda, Y. Miyamoto, *J. Macromol. Sci. B* 45 (2006) 1141.
- [114] M.V. Massa, K. Dalnoki-Veress, J.A. Forrest, *Eur. Phys. J. E* 11 (2003) 191.
- [115] S. Sawamura, H. Miyaji, K. Izumi, S.J. Sutton, Y. Miyamoto, *J. Phys. Soc. Jpn.* 67 (1998) 3338.
- [116] K. Jeon, R. Krishnamoorti, *Macromolecules* 41 (2008) 7131.
- [117] Y. Wang, C. Chan, K. Ng, L. Li, *Macromolecules* 41 (2008) 2548.
- [118] T. Yamamoto, K. Nozaki, A. Yamaguchi, N. Urakami, *J. Chem. Phys.* 127 (2007) 154704.
- [119] O.E. Farrance, R.A.L. Jones, J.K. Hobbs, *Polymer* 50 (2009) 3730.
- [120] A. Toda, K. Taguchi, H. Kajioka, *Macromolecules* 41 (2008) 7505.
- [121] Y. Duan, Y. Jiang, S. Jiang, L. Li, S. Yan, J.M. Schultz, *Macromolecules* 37 (2004) 9283.
- [122] Y. Saito, *Statistical Physics of Crystal Growth*, World Scientific, Singapore, 1996.
- [123] E. Brener, H. Müller-Krumbhaar, D. Temkin, *Europhys. Lett.* 17 (1992) 535.
- [124] E. Brener, H. Müller-Krumbhaar, D. Temkin, T. Abel, *Physica A* 249 (1998) 73.
- [125] E. Brener, H. Müller-Krumbhaar, D. Temkin, *Phys. Rev. E* 54 (1996) 2714.
- [126] T. Ihle, H. Müller-Krumbhaar, *Phys. Rev. E* 49 (1994) 2972.
- [127] L. Gránáys, T. Pusztai, T. Börzsönyi, J.A. Warren, J.F. Douglas, *Nat. Mater.* 3 (2004) 645.
- [128] K. Taguchi, H. Miyaji, K. Izumi, A. Hoshino, Y. Miyamoto, R. Kokawa, *J. Macromol. Sci. B* 41 (2002) 1033.
- [129] D.S. Zhu, Y.X. Liu, E.Q. Chen, M. Li, S.Z. Cheng, *Acta Polym. Sin.* (2006) 1125.
- [130] G. Reiter, J.U. Sommer, *J. Chem. Phys.* 112 (2000) 4376.
- [131] J.U. Sommer, G. Reiter, *J. Chem. Phys.* 112 (2000) 4384.
- [132] Y. Saito, T. Ueta, *Phys. Rev. A* 40 (1989) 3408.
- [133] H. Xu, R. Matkar, T. Kyu, *Phys. Rev. E* 72 (2005) 11804.
- [134] V.A. Bogoyavlenskiy, *Phys. Rev. E* 64 (2001) 66303.
- [135] V.A. Bogoyavlenskiy, N.A. Chernova, *Phys. Rev. E* 61 (2000) 1629.
- [136] V.A. Bogoyavlenskiy, N.A. Chernova, *Phys. Rev. E* 61 (2000) 5422.
- [137] E. Brener, H. Levine, Y. Tu, *Phys. Rev. Lett.* 66 (1991) 1978.
- [138] T.A. Witten, L.M. Sander, *Phys. Rev. Lett.* 47 (1981) 1400.
- [139] M. Uwaha, Y. Saito, *Phys. Rev. A* 40 (1989) 4716.
- [140] N. Goldenfeld, *J. Cryst. Growth* 84 (1987) 601.
- [141] J.J. Point, A.J. Kovacs, *Macromolecules* 13 (1980) 399.
- [142] E.G. Putra, G. Ungar, *Macromolecules* 36 (2003) 5214.
- [143] A. Rottele, T. Thurn-Albrecht, J.U. Sommer, G. Reiter, *Macromolecules* 36 (2003) 1257.
- [144] M. Massa, J. Carvalho, K. Dalnoki-Veress, *Eur. Phys. J. E* 12 (2003) 111.
- [145] M.M. Despotopoulou, C.W. Frank, R.D. Miller, J.F. Rabolt, *Macromolecules* 29 (1996) 5797.
- [146] M.M. Despotopoulou, R.D. Miller, J.F. Rabolt, C.W. Frank, *J. Polym. Sci. B* 34 (1996) 2335.
- [147] D.S. Zhu, X.X. Shou, Y.X. Liu, E.Q. Chen, S.Z. Di Cheng, *Front. Chem. China* 2 (2007) 174.
- [148] J.K. Hobbs, M.J. Miles, *Macromolecules* 34 (2001) 353.
- [149] H. Schönherr, C.W. Frank, *Macromolecules* 36 (2003) 1199.
- [150] J.M. Schultz, *Macromolecules* 29 (1996) 3022.
- [151] Y. Zhang, J. Zhang, Y. Lu, Y. Duan, S. Yan, D. Shen, *Macromolecules* 37 (2004) 2532.
- [152] Y. Wang, C. Chan, Y. Jiang, L. Li, K. Ng, *Macromolecules* 40 (2007) 4002.
- [153] L. Mandelkern, A.S. Posner, A.F. Diorio, D.E. Roberts, *J. Appl. Phys.* 32 (1961) 1509.
- [154] E.W. Fischer, *Angew. Chem. Int. Edit.* 1 (1962) 488.
- [155] B. Wunderlich, *Macromolecular Physics*, vol. 2, Academic Press, New York, 1976.
- [156] S.J. Organ, J.K. Hobbs, M.J. Miles, *Macromolecules* 37 (2004) 4562.
- [157] J. Duan, B. Guo, *J. Polym. Sci. B* 47 (2009) 1492.
- [158] X. Zhai, G. Zhang, Z. Ma, X. Tang, W. Wang, *Macromol. Chem. Phys.* 208 (2007) 651.
- [159] D.S. Zhu, Y.X. Liu, A.C. Shi, E.Q. Chen, *Polymer* 47 (2006) 5239.
- [160] X.M. Zhai, W. Wang, Z.P. Ma, X.J. Wen, F. Yuan, X.F. Tang, B.L. He, *Macromolecules* 38 (2005) 1717.
- [161] G. Reiter, G. Castelein, J.U. Sommer, *Phys. Rev. Lett.* 86 (2001) 5918.
- [162] J.U. Sommer, G. Reiter, *Adv. Polym. Sci.* 200 (2006) 1.
- [163] J.U. Sommer, G. Reiter, *Thermochim. Acta* 432 (2005) 135.
- [164] G. Reiter, *J. Polym. Sci. B* 41 (2003) 1869.
- [165] A.J. Kovacs, A. Gonthier, C. Straupe, *J. Polym. Sci. Polym. Symposia* 50 (1975) 283.
- [166] A. Peterlin, *Polymer* 6 (1965) 25.
- [167] A. Peterlin, *J. Polym. Sci. Part B: Polym. Lett.* 1 (1963) 279.
- [168] J.J. Weeks, *J. Res. Natl. Bur. Stand. Sect. A* 67 (1963) 441.